J. Appl. Comput. Mech., 12(3) (2026) 828-847
DOI: 10.22055/jacm.2025.48450.5241

ISSN: 2383-4536
jacm.scu.ac.ir

Shahid Chamran University of Ahvaz

Journal of Applied and Computational Mechanics

Research Paper

Mechanical Stability of SiC/C Double- and Triple-Walled Nanotubes under Compression: Implications for Structural Integrity in Battery Electrodes

Guanghui Liu[1], Liang Yuan[2,3]

[1] School of Intelligent Manufacturing, Luohe Food Engineering Vocational University, Luohe, Henan, 462300, China, Email: Guanghui.liu84@outlook.com

[2] College of Architecture and Civil Engineering, Xinyang Normal University, Xinyang, Henan 464000, China, Email: r.h.sea857@gmail.com

[3] Henan New Environmentally-Friendly Civil Engineering Materials Engineering Research Center, Xinyang Normal University, Xinyang, Henan 464000, China

Received May 11 2025; Revised September 26 2025; Accepted for publication October 04 2025.
✉ Corresponding author: L. Yuan (r.h.sea857@gmail.com)

Abstract. This study presents a comprehensive finite element (FE) analysis of the critical compressive buckling forces in concentric silicon carbide (SiC) and carbon (C) multi-walled nanotubes (MWNTs), focusing on their relevance to high-performance battery electrode applications. The analysis compares double-walled (DWNTs) and triple-walled nanotubes (TWNTs) across variations in wall sequence, length, radius, and chirality (armchair vs. zigzag). Results indicate that zigzag-configured MWNTs exhibit superior axial stability compared to their armchair counterparts, due to enhanced bond alignment. TWNTs, particularly those with more carbon layers (e.g., C-C-C), demonstrate significantly higher buckling resistance, making them ideal candidates for mechanically robust nanostructures in energy storage devices. The outermost wall properties significantly influence the buckling behavior in DWNTs, particularly at higher aspect ratios where global buckling modes dominate. While chirality effects are most pronounced at lower aspect ratios, radius-dependent effects show the opposite trend, with smaller radii providing enhanced stability primarily in short, low-aspect-ratio configurations. These insights inform the design of next-generation battery electrodes where nanostructural integrity under cyclic mechanical and electrochemical stresses is critical for long-term performance and reliability.

Keywords: Finite element method; Buckling behavior; Silicon carbide nanotubes; Multi-walled nanotubes; Chirality; Mechanical stability.

1. Introduction

Silicon carbide (SiC) has gained prominence as an advanced material for extreme-environment applications, owing to its exceptional mechanical robustness, superior thermal conductivity, and adjustable electronic properties [1-3]. These distinctive traits make SiC an optimal choice for aerospace components, energy storage solutions, including high-performance battery electrodes, and semiconductor technologies [4-6]. Recent advances in fabricating and analyzing SiC nanostructures, such as nanotubes (SiCNTs) and nanosheets (SiCNSs), have sparked considerable interest due to their unparalleled performance and versatility in next-generation applications [7-10]. Studies on their mechanical, thermal, and electronic behavior suggest they could surpass conventional carbon-based nanomaterials in specific high-performance settings, particularly where structural integrity under cyclic mechanical stress is critical, such as in lithium-ion battery electrodes [11-15].

The mechanical properties of SiC nanostructures, particularly their elastic modulus, tensile strength, and buckling behavior, have been a focal point of research. Molecular dynamics (MD) simulations and experimental studies have shown that SiCNTs exhibit high elastic moduli, ranging from 465 GPa to 540 GPa, depending on wall thickness and diameter [16-18]. For instance, Pan and Si [16] reported that the elastic modulus of SiCNTs enhances with wall thickness, highlighting the importance of structural parameters in determining mechanical performance. Similarly, Wang et al. [17] studied the compressive and tensile properties of twinned SiC nanowires, revealing their elastically linear behavior followed by brittle fracture, a critical consideration for high-stress applications like battery electrodes subjected to repeated lithiation/delithiation cycles. The compressibility of periodically twinned silicon carbide (SiC) nanowires was investigated through in situ high-pressure X-ray diffraction by Lin et al. [18]. The results revealed a bulk modulus of 316 GPa for the twinned SiC nanowires, which is approximately 20–40% higher than values previously reported for other SiC morphologies. This study provided direct experimental evidence that twinned structures significantly enhance the elastic properties of SiC at the nanoscale, corroborating earlier molecular dynamics simulations that predicted strengthening effects due to twin boundaries and stacking faults. Both experimental data and simulations suggest that nanoscale twinning represents a promising approach for engineering the mechanical properties of nanostructured materials.

Published online: October 12 2025

Buckling behavior, a key mechanical property for nanostructures under compressive loads, has also been extensively studied. Setoodeh et al. [19] used MD simulations to identify two distinct buckling modes in SiCNTs: local and global buckling. Ansari et al. [20] further explored the buckling behavior of SiCNTs using finite element (FE) methods, demonstrating that the critical buckling force is influenced by the nanotube's length and diameter. These studies have provided valuable insights into the stability of SiCNTs under compressive loads, which is crucial for their application in nanoscale devices, composites, and energy storage systems where mechanical degradation limits longevity [21-23].

Despite the extensive research on SiC nanostructures, the mechanical stability of multi-walled SiC and carbon (C) nanotubes under compressive loads remains underexplored. Multi-walled nanotubes (MWNTs) offer enhanced mechanical properties due to interlayer interactions, making them suitable for high-load applications such as conductive scaffolds in battery electrodes [24-26]. For example, in battery systems, MWNTs must resist deformation under electrochemical cycling, where compressive forces can lead to structural failure and capacity fade. Shim et al. [24] employed N_2-assisted molecular dynamics simulations to probe the axial collapse resistance of dual-walled SiCNTs. Their experimental framework incorporated four distinct chiral configurations, with special emphasis on nanotube aspect ratios as a governing factor for buckling dynamics. During compressive failure, an unprecedented interfacial phenomenon emerged: atomic bonding between inner and outer wall layers at buckling sites, accompanied by a reversible sp2-to-sp3 hybridization shift in SiC bonds. This transformation—attributed to SiC's intrinsic self-repair mechanism—mirrored the energetic profile of zinc blende SiC, as validated by strain energy hysteresis and radial distribution function (RDF) anomalies.

Asmadi et al. [25] explored the thermal property enhancement of epoxy composites reinforced with hybrid nanofillers, consisting of multi-walled carbon nanotubes (MWCNTs) and silicon carbide nanoparticles (SiCs), fabricated via solution mixing. The incorporation of 4 vol.% MWCNTs doubled the thermal conductivity compared to pure epoxy, while a hybrid filler combination of 3 vol.% MWCNTs and 1 vol.% SiCs achieved an even higher value of 0.48 W/mK, demonstrating synergistic effects and effective conductive pathway formation. Besides, molecular dynamics simulations revealed that the temperature-dependent expansion of cellulose reduces stress transfer at the filler-matrix interface, significantly impacting the tensile properties of silicon carbide nanotube (SiCNT)- and carbon nanotube (CNT)-reinforced cellulose composites. While single-walled CNTs enhance tensile strength and toughness, multi-walled CNTs improve stiffness, and hybridization of SiCNTs with CNTs enhances structural stability and performance across varying temperatures [26].

Size-dependent effects become increasingly significant at the nano-scale. Different modeling frameworks, particularly nonlocal elasticity theories, have been extensively developed to capture small-scale phenomena that classical theories may overlook. The nonlocal elasticity theory, first proposed by Eringen, assumes that stress at a reference point depends on the strain field at all points in the body, effectively incorporating size effects through a characteristic length parameter [27, 28]. This approach has been successfully applied to analyze buckling behavior of single-walled [27, 29], double-walled [28], and triple-walled carbon nanotubes [27], demonstrating that nonlocal effects can significantly influence critical buckling loads, particularly for nanotubes with smaller length-to-diameter ratios. Recent advances have extended these theories to curved nanostructures [30, 31] and developed efficient computational methods such as the initial value method combined with approximate transfer matrix approaches [30-32]. While these nonlocal theories provide important theoretical insights into size-dependent mechanics, the classical FEM approach adopted in this study offers computational efficiency and established validation frameworks that are well-suited for the systematic parametric analysis of hybrid SiC/C multi-walled nanotubes presented herein.

Recent developments in computational nanomechanics have demonstrated the power of hybrid approaches that combine quantum mechanical calculations with molecular mechanics methods to study nanotube behavior. Mirnezhad et al. [33] pioneered the investigation of quantum effects of fine scaling on CNT buckling behavior under both axial and torsional loading conditions, revealing significant size-dependent variations in critical buckling strains that are not captured by purely continuum approaches. Similarly, Nickabadi et al. [34] successfully applied three-dimensional finite element methods based on molecular mechanics to study vibrational properties of double-walled silicon carbide nano-cones, while Ansari and coworkers [35, 36] have extensively utilized DFT-based finite element approaches to characterize mechanical properties of various nanotube structures including phosphorene nanotubes. These hybrid methodologies bridge the gap between atomic-scale quantum effects and continuum mechanics, enabling more accurate predictions of mechanical behavior across different length scales. The integration of density functional theory calculations with structural mechanics approaches has proven particularly valuable for determining force constants and material properties that reflect the true quantum mechanical nature of interatomic bonding, thereby providing a more fundamental understanding of nanotube mechanical behavior than traditional continuum models [37].

Advances in computational nanomechanics have primarily focused on homogeneous nanotube systems, leaving significant gaps in understanding heterogeneous configurations. While Nickabadi et al. [34] conducted finite element investigations of double-walled SiC nano-cones, and Mercan & Civalek [38] performed molecular dynamics studies on SiC nanotube buckling for gas sensing applications, these studies did not address the complex interlayer dynamics in concentric SiC/C hybrid systems. The unique challenge in hybrid SiC/C nanotubes lies in the asymmetric interlayer interactions, where van der Waals forces between dissimilar materials (SiC-C interfaces) differ substantially from those in homogeneous systems (C-C or SiC-SiC interfaces), creating heterogeneous stress distributions that conventional single-material models cannot capture. Furthermore, recent progress in battery electrode design has highlighted the critical importance of mechanical stability under cyclic loading, where Fan et al. [39] demonstrated that SiC nanostructures in lithium-ion batteries require enhanced interfacial bonding to prevent capacity fade due to mechanical degradation. The present work addresses these gaps by developing a comprehensive finite element framework specifically designed for concentric SiC/C multi-walled nanotubes, incorporating differentiated van der Waals interactions and systematic analysis of wall sequence effects—aspects that have not been systematically investigated in prior computational studies of hybrid nanotube systems.

In this paper, the buckling behavior of concentric SiC/C MWNTs, which combine the mechanical strength of SiC with the flexibility of carbon, has not been thoroughly investigated. Understanding the critical compressive forces and stability characteristics of these hybrid nanostructures is essential for their practical implementation in nanotechnology, particularly in designing durable electrodes for next-generation batteries. To address the existing gap in understanding the mechanical stability of hybrid SiC/C nanostructures, this study employs a finite element (FE) approach to investigate the buckling behavior of concentric SiC and C multi-walled nanotubes (MWNTs) under axial compression. The analysis focuses on double-walled (DWNTs) and triple-walled (TWNTs) configurations with systematically varied wall orders (e.g., SiC-C, C-SiC-C), chiralities (armchair and zigzag), and geometric parameters (length, radius). By evaluating the interplay between material composition, atomic structure, and interlayer interactions, this work aims to establish design principles for enhancing the compressive stability of SiC/C hybrid nanotubes. The findings will contribute to the development of high-performance nanomaterials for energy storage applications, where mechanical stability under compression is as critical as electrochemical performance.

Table 1. Interatomic Force Constants and Equilibrium Bond Lengths.

	C-C [45]	Si-C [20]
k_r	$6.52 \times 10^{-7}\,\mathrm{N/nm}$	$4.17 \times 10^{-7}\,\mathrm{N/nm}$
k_θ	$8.76 \times 10^{-10}\,\mathrm{Nnm/rad^2}$	$8.42 \times 10^{-10}\,\mathrm{Nnm/rad^2}$
k_τ	$2.78 \times 10^{-10}\,\mathrm{Nnm/rad^2}$	$1.505 \times 10^{-9}\,\mathrm{Nnm/rad^2}$
L	1.421Å	1.786 Å

While this finite element approach provides valuable insights into the mechanical stability of SiC/C nanotubes, several important limitations must be acknowledged. The current structural mechanics-based model treats nanotubes as purely mechanical structures under static loading conditions and cannot capture dynamic effects relevant to battery electrode applications. Specifically, the model does not account for electrochemical processes such as lithium intercalation/deintercalation during charge-discharge cycles, temperature-induced changes in material properties, chemical potential variations affecting bond strengths, or the generation of electrochemical stresses during battery operation. Additionally, the model assumes perfect crystal structures without defects, uniform material properties, and quasi-static loading conditions.

The force constants and material properties used in the beam-spring element representation are derived from equilibrium molecular configurations and may not accurately reflect the altered bonding environments during electrochemical cycling. Furthermore, the Lennard-Jones potential used to model van der Waals interactions between nanotube walls assumes constant parameters that may vary with temperature and chemical environment in real battery systems. Therefore, while the present study establishes fundamental mechanical stability principles for SiC/C multi-walled nanotubes under compression, future multiphysics approaches incorporating electrochemical-mechanical coupling, temperature effects, and dynamic loading conditions will be necessary to fully understand their behavior in practical energy storage applications. The findings presented here serve as a foundation for such advanced modeling efforts and provide design guidelines for the mechanical aspects of nanotube-based electrode structures.

2. Molecular Structural Model

In this section, the elemental properties of the utilized three-dimensional FE method are obtained. For this purpose, first, the expressing of the total energy in the structural mechanics is considered as [40, 41]:

$$U_{total} = \sum U_r + \sum U_\theta + \sum U_\emptyset + \sum U_\omega + \sum U_{vdW} \tag{1}$$

where the following relation is used to express the bond stretching energy, U_r [42, 43]:

$$U_r = \frac{1}{2}k_r(r - r_0)^2 = \frac{1}{2}k_r(\Delta r)^2 \tag{2}$$

The bond bending energy, U_θ, is stated as:

$$U_\theta = \frac{1}{2}k_\theta(\theta - \theta_0)^2 = \frac{1}{2}k_\theta(\Delta\theta)^2 \tag{3}$$

The torsional term is considered as the summation of the dihedral angle torsion, $U_\emptyset$, and out-of plane torsion, U_ω, energies and is expressed as:

$$U_\tau = U_\emptyset + U_\omega = \frac{1}{2}k_\tau(\Delta\emptyset)^2 \tag{4}$$

In Eqs. (2) to (4), the bond stretching, bond bending and bond torsion force constants are respectively shown by k_r, k_θ and k_τ. Besides, Δr, $\Delta\theta$ and $\Delta\emptyset$ are, respectively, used to denote the variations of the bond length, bond angle and dihedral angle form the initial position. Moreover, due to small portion of the nonbonding interaction compared to other terms in Eq. (1), U_{vdW} is disregarded. By modeling chemical bonds as beam elements with circular cross-sections, the associated potential energies can be formulated as follows:

$$U_A = \frac{1}{2}\int_0^L \frac{N^2}{EA}dL = \frac{1}{2}\frac{N^2L}{EA} = \frac{1}{2}\frac{EA}{L}(\Delta L)^2 \tag{5}$$

$$U_M = \frac{1}{2}\int_0^L \frac{M^2}{EI}dL = \frac{2EI}{L}\alpha^2 = \frac{1}{2}\frac{EI}{L}(2\alpha)^2 \tag{6}$$

$$U_T = \frac{1}{2}\int_0^L \frac{T^2}{GJ}dL = \frac{1}{2}\frac{T^2L}{GJ} = \frac{1}{2}\frac{GJ}{L}(\Delta\beta)^2 \tag{7}$$

The geometric properties—moment of inertia (I), polar moment of inertia (J), and cross-sectional area (A)—are defined as $I = \frac{\pi d^4}{64}$, $J = \frac{\pi d^4}{32}$, and $A = \frac{\pi d^2}{4}$, where d represents diameter. Besides, the applied loads are shown by N, stretching force, M, bending moment and T, torque. E and G are used to denote the elastic and shear moduli, respectively. Now, Eqs. (2) to (4) are equated to Eqs. (5) to (7). Therefore:

$$\begin{aligned} \frac{EA}{L} &= k_r \\ \frac{EI}{L} &= k_\theta \\ \frac{GJ}{L} &= k_\tau \end{aligned} \tag{8}$$

Table 2. ε and σ constants for C-C, and Si-C pairs [47].

	C-C	Si-C
ε (NÅ)	3.4	3.1
σ (Å)	5.97×10^{-12}	1.5186×10^{-11}

To obtain the elemental properties, one should substitute the expressions of the A, I and J into the above equations [31]:

$$d = 4\sqrt{\frac{k_\theta}{k_r}}, \qquad E = \frac{k_r^2 L}{4\pi k_\theta}, \qquad G = \frac{k_r^2 k_\tau L}{8\pi k_\theta^2} \tag{9}$$

The interatomic force constants for Si-C and C-C bonds, as documented in Table 1, serve as fundamental inputs for Eqs. (9). So $d_{C-C} = 1.466$ Å, $E_{C-C} = 5.488 \times 10^{-8}\, {}^{N}/_{\text{Å}^2}$, $G_{C-C} = 8.701 \times 10^{-9}\, {}^{N}/_{\text{Å}^2}$, $d_{Si-C} = 1.7971$Å, $E_{Si-C} = 2.9372 \times 10^{-8}\, {}^{N}/_{\text{Å}^2}$, $G_{Si-C} = 2.6256 \times 10^{-8}\, {}^{N}/_{\text{Å}^2}$ [44].

Using the Lennard-Jones potential function to simulate the nonbonding van der Waals interactions, the spring elements are employed to model the nonbonding interaction between the atoms located on different walls. The stiffness of the elements are obtained as [46]:

$$k_{vdw} = 24\varepsilon\left(26\frac{\sigma^{12}}{R^{14}} - 7\frac{\sigma^6}{R^8}\right) \tag{10}$$

where ε and σ are the Lennard-Jones constants (see Table 2). Besides, the interatomic distance is shown by R. When the distance between two atoms located on different walls is $R < 2.5\ \sigma$, a spring element is considered between them that depending on their types, its stiffness is obtained by substituting the values given in Table 2 into Eq. (10). Besides, R is the interatomic distance. The spring elements are considered between atoms whose distance is smaller than $2.5\ \sigma$.

Figure 1 illustrates a schematic representation of the beam and spring elements employed in the finite element (FE) model to simulate the buckling behavior of concentric silicon carbide (SiC) and carbon (C) multi-walled nanotubes (MWNTs). The diagram depicts a simplified structural model where covalent bonds between atoms are represented as beam elements with circular cross-sections, characterized by their elastic modulus (E), shear modulus (G), and geometric properties such as cross-sectional area (A), moment of inertia (I), and polar moment of inertia (J). These beam elements account for the stretching, bending, and torsional interactions within the nanotube walls, as derived from the molecular structural mechanics approach. Additionally, the figure includes spring elements, which model the nonbonding van der Waals interactions between atoms located on different walls of the MWNTs. The stiffness of these spring elements is calculated using the Lennard-Jones potential, with parameters specific to the interatomic distances and types (e.g., C-C or Si-C pairs). The schematic visually distinguishes between the beam elements, aligned along the bond directions, and the spring elements, connecting atoms across the inter-wall spacing, providing a clear conceptual framework for the FE-based buckling analysis presented in the study.

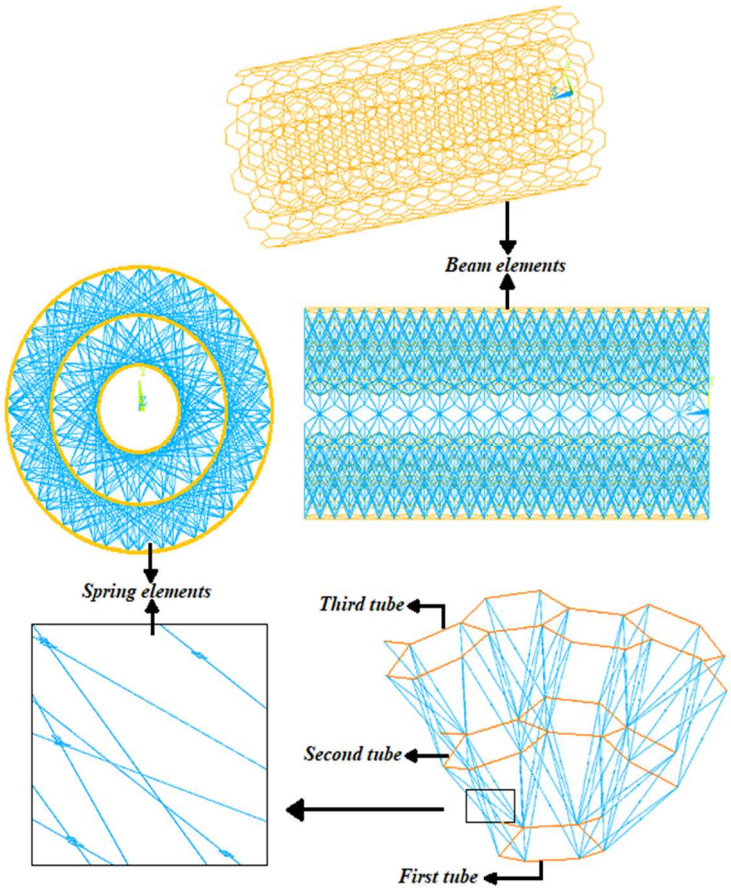

Fig. 1. Schematic representation of beam and spring elements used in the analysis.

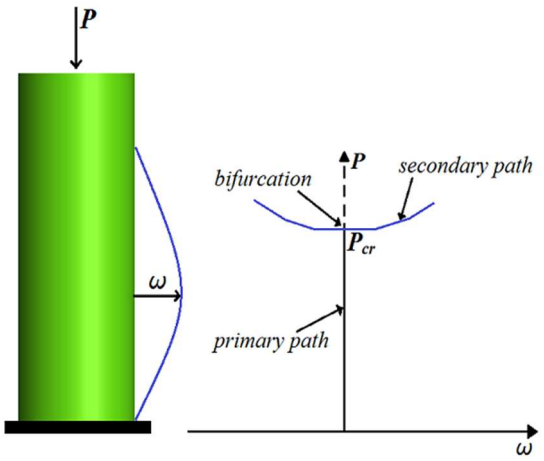

Fig. 2. Representation of the bifurcation point.

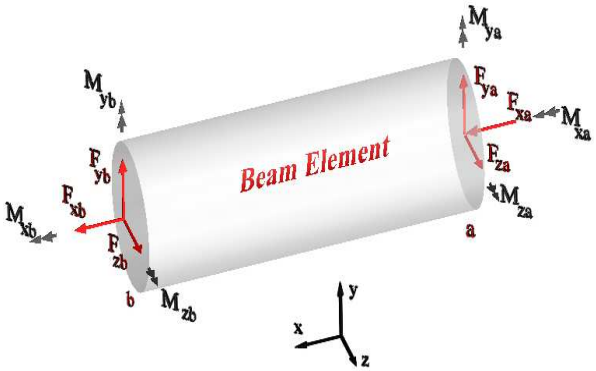

Fig. 3. Schematics of the loadings on a beam element.

3. Finite Element Method (FEM) for Buckling Analysis of Nanostructures

Employing bifurcation approach to compute the buckling force of the MWNTs. As illustrated in Fig. 2, this method examines a perfect column subjected to axial compressive loading. Figure 2 presents a conceptual diagram illustrating the bifurcation point in the buckling analysis of a perfect column subjected to an axial compressive force, as utilized in the finite element (FE) investigation of concentric silicon carbide (SiC) and carbon (C) multi-walled nanotubes (MWNTs). The figure features a force-deformation graph alongside a schematic of the column, highlighting the transition from a stable to an unstable state. The primary path, depicted as a straight line, represents the initial linear response of the column under compression, where no transverse deformation occurs prior to buckling. At the bifurcation point, marked as the intersection of the primary and secondary paths, the column reaches its critical compressive load, beyond which a small increase in force results in significant transverse deformation. This secondary, or postbuckling, path is shown as a diverging curve, indicating the onset of instability. The diagram effectively conveys the theoretical foundation of the bifurcation approach employed in the study, linking the mechanical behavior of the column to the computed critical buckling forces of the MWNTs, thus providing a visual aid for understanding the stability characteristics analyzed in the research.

Figure 3 provides a schematic representation of the loadings applied to a beam element within the finite element (FE) framework used to analyze the buckling behavior of concentric silicon carbide (SiC) and carbon (C) multi-walled nanotubes (MWNTs). The diagram illustrates a single beam element subjected to a combination of mechanical forces and moments, including an axial stretching force (N), bending moments (M) acting about the y- and z-axes, and a torque (T) inducing torsional deformation. These loads are depicted as arrows and curved lines at the ends of the beam, with annotations indicating their directions and points of application. The beam, modeled with a circular cross-section, is characterized by its length (L) and material properties such as elastic modulus (E) and shear modulus (G), which govern its response to the applied forces. Accompanying the schematic is a set of equations defining parameters (a through r) that quantify the contributions of these loads to the geometric stiffness matrix, essential for capturing the buckling instability in the FE simulations. This figure serves as a critical visual tool to elucidate the mechanical interactions modeled in the study, linking the theoretical load configurations to the stability analysis of the MWNTs.

In the initial phase of analysis, the elemental stiffness matrix S is derived through the superposition of elastic and geometric stiffness components. The formulation considers:

- $[K]_b^e$: Stiffness matrix for beam elements
- $[K]_s^e$: Stiffness matrix for spring elements

The elastic stiffness matrix is then expressed as:

$$[K]^e = [K]_b^e + [K]_s^e \tag{11}$$

in which $[K]_b^e$ is obtained as:

$$[K]_b^e = \begin{bmatrix} [K_{ii}]_b^e & [K_{ij}]_b^e \\ [K_{ji}]_b^e & [K_{jj}]_b^e \end{bmatrix} \tag{12}$$

where,

$$[K_{ii}]_b^e = \begin{bmatrix} EA/L & 0 & 0 & 0 & 0 & 0 \\ 0 & 12EI_x/L^3 & 0 & 0 & 0 & 6EI_x/L^2 \\ 0 & 0 & 12EI_y/L^3 & 0 & -6EI_y/L^2 & 0 \\ 0 & 0 & 0 & GJ/L & 0 & 0 \\ 0 & 0 & -6EI_y/L^2 & 0 & 4EI_y/L & 0 \\ 0 & 6EI_x/L^2 & 0 & 0 & 0 & 4EI_x/L \end{bmatrix} \tag{13}$$

$$[K_{ij}]_b^e = \begin{bmatrix} -EA/L & 0 & 0 & 0 & 0 & 0 \\ 0 & -12EI_x/L^3 & 0 & 0 & 0 & 6EI_x/L^2 \\ 0 & 0 & -12EI_y/L^3 & 0 & -6EI_y/L^2 & 0 \\ 0 & 0 & 0 & -GJ/L & 0 & 0 \\ 0 & 0 & 6EI_y/L^2 & 0 & 2EI_y/L & 0 \\ 0 & -6EI_x/L^2 & 0 & 0 & 0 & 2EI_x/L \end{bmatrix} \tag{14}$$

$$[K_{jj}]_b^e = \begin{bmatrix} EA/L & 0 & 0 & 0 & 0 & 0 \\ 0 & 12EI_x/L^3 & 0 & 0 & 0 & -6EI_x/L^2 \\ 0 & 0 & 12EI_y/L^3 & 0 & 6EI_y/L^2 & 0 \\ 0 & 0 & 0 & GJ/L & 0 & 0 \\ 0 & 0 & 6EI_y/L^2 & 0 & 4EI_y/L & 0 \\ 0 & -6EI_x/L^2 & 0 & 0 & 0 & 4EI_x/L \end{bmatrix} \tag{15}$$

and $[K_{ji}]_b^e = ([K_{ij}]_b^e)^T$. Moreover, the elastic stiffness matrix associated with the spring element is expressed as:

$$[K]_s^e = \begin{bmatrix} [K_{ii}]_s^e & [K_{ij}]_s^e \\ [K_{ji}]_s^e & [K_{jj}]_s^e \end{bmatrix} \tag{16}$$

where,

$$[K_{ii}]_s^e = [K_{jj}]_s^e = \begin{bmatrix} [A] & [O] \\ [O] & [O] \end{bmatrix} \tag{17}$$

where $[O] = \begin{bmatrix} 0 & 0 & 0 \\ 0 & 0 & 0 \\ 0 & 0 & 0 \end{bmatrix}$ and:

$$[A] = \begin{bmatrix} \alpha & 0 & 0 \\ 0 & 0 & 0 \\ 0 & 0 & 0 \end{bmatrix} \tag{18}$$

and,

$$\alpha = \ k_{vdw} = 24\varepsilon \left(26 \frac{\sigma^{12}}{R^{14}} - 7 \frac{\sigma^6}{R^8} \right) \tag{19}$$

which is the second derivative of the Lennard-Jones potential function with respect the interatomic distance (R) and ε and σ are the Lennard-Jones coefficient. Besides:

$$[K_{ij}]_s^e = -[K_{ii}]_s^e \tag{20}$$

The following equation is used to obtain the geometric stiffness matrix:

$$K^g = \begin{bmatrix} [K_{ii}]^g & [K_{ij}]^g \\ [K_{ji}]^g & [K_{jj}]^g \end{bmatrix} \tag{21}$$

where $[K_{ji}]^g = ([K_{ij}]^g)^T$ and:

$$[K_{ii}]^g = \begin{bmatrix} a & 0 & 0 & 0 & -d & -e \\ & b & 0 & d & g & k \\ & & c & e & h & g \\ & & & f & i & l \\ & Sym. & & & j & 0 \\ & & & & & m \end{bmatrix} \tag{22}$$

$$[K_{ij}]^g = \begin{bmatrix} -a & 0 & 0 & 0 & -n & -o \\ 0 & -b & 0 & n & -g & k \\ 0 & 0 & -c & o & -h & -g \\ 0 & -d & -e & -f & -i & -l \\ d & -g & h & -i & p & -q \\ e & -k & -g & -l & q & r \end{bmatrix} \tag{23}$$

$$[K_{jj}]^g = \begin{bmatrix} a & 0 & 0 & 0 & n & o \\ & b & 0 & -n & g & -k \\ & & c & -o & h & g \\ & & & f & i & l \\ & Sym. & & & j & 0 \\ & & & & & m \end{bmatrix} \tag{24}$$

Based on Fig. 3, the following relations can be used to obtain parameters a to r:

$$a=\frac{F_{xb}}{L}, b=c=\frac{6F_{xb}}{5L}+\frac{12F_{xb}I}{AL^3}, d=\frac{M_{ya}}{L}, e=\frac{M_{za}}{L}, f=\frac{F_{xb}J}{AL}, g=\frac{M_{xb}}{L}, h=k=\frac{F_{xb}}{10}+\frac{6F_{xb}I}{AL^2}, i=\frac{M_{za}+M_{zb}}{L},$$
$$j=m=\frac{12F_{xb}}{15}+\frac{4F_{xb}I}{AL}, l=-\frac{M_{ya}+M_{yb}}{6}, n=\frac{M_{yb}}{L}, o=\frac{M_{zb}}{L}, p=r=-\frac{F_{xb}}{30}+\frac{2F_{xb}I}{AL}, q=-\frac{M_{xb}}{L} \tag{25}$$

The elemental stiffness matrix is assembled to obtain the global stiffness matrix. If the external applied load and assembled stiffness matrix are expressed as:

$$P=\lambda P^* \tag{26}$$

$$K_G=\lambda K_G^* \tag{27}$$

where λ, P^* and K_G^* are a constant, the relative magnitudes of the applied forces and the geometric stiffness matrix of P^*, the following equation can be written:

$$(K_E+\lambda K_G^*)U=\lambda P^* \tag{28}$$

where the K_E is considered to be constant for a wide range of the displacement (U). At the bifurcation, one should set:

$$|K_E+\lambda K_G^*|=0 \tag{29}$$

The critical compressive force is obtained as:

$$P_{cr}=\lambda_{cr}P^* \tag{30}$$

in which λ_{cr} is the critical value of the λ which is obtained by solving Eq. (29).

3.1. Sensitivity analysis for beam-spring FE model

Figure 4 presents a comprehensive parameter sensitivity analysis for the developed beam-spring finite element (FE) model, illustrating how variations in key input parameters affect the predicted buckling force of the multi-walled nanotubes (MWNTs). The figure consists of six subplots, each showing the percentage change in buckling force as a function of the percentage variation in a specific model parameter, for different aspect ratios (L/D = 2, 4, 6, 8, 10). The parameters investigated include the Young's modulus of C-C bonds (E_{C-C}), Young's modulus of SiC bonds (E_{Si-C}), diameter of C-C bonds (d_{C-C}), diameter of SiC bonds (d_{Si-C}), van der Waals stiffness coefficient for C-C interactions, and van der Waals stiffness coefficient for SiC-C interactions.

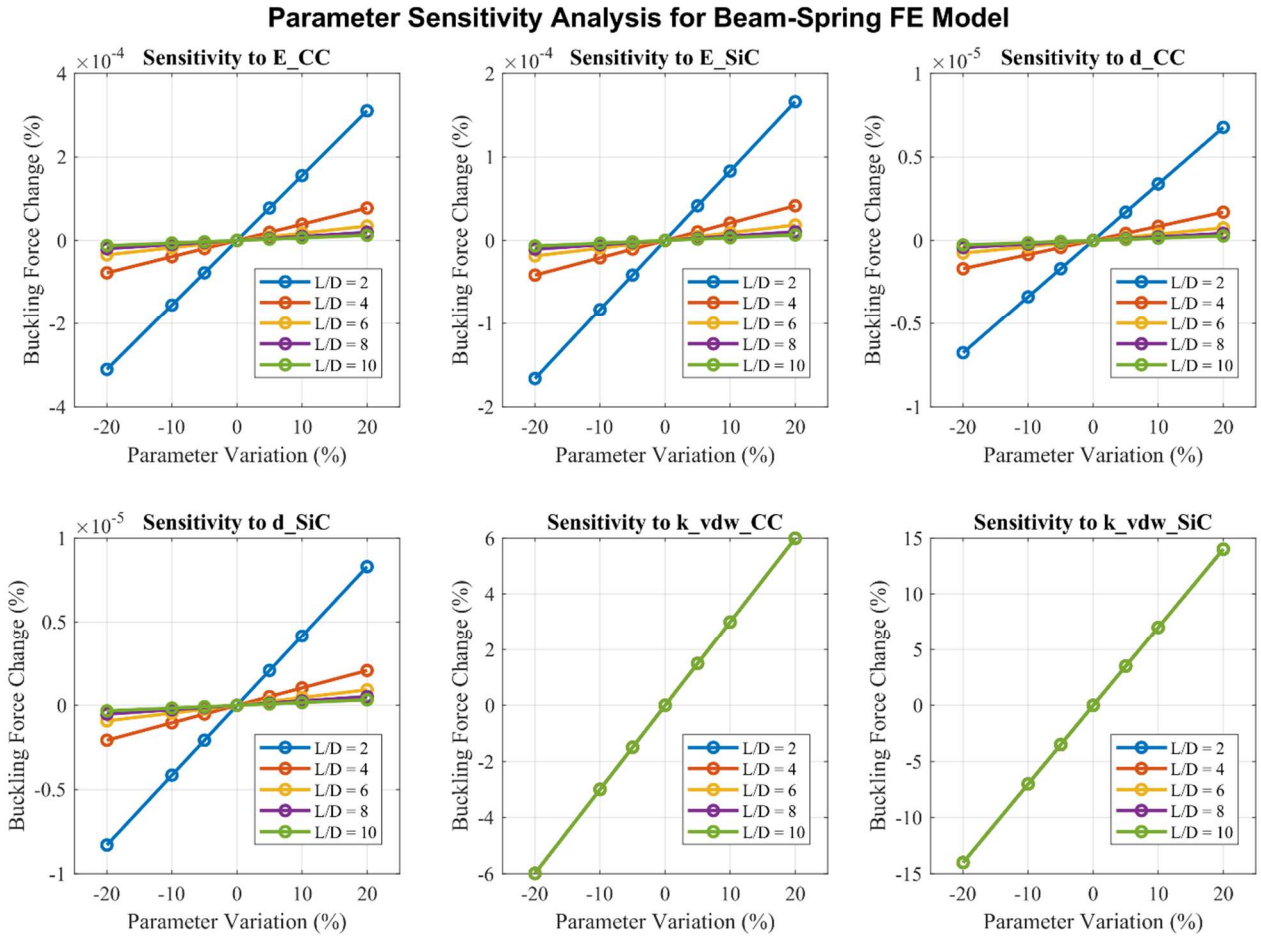

Fig. 4. Comprehensive parameter sensitivity analysis for the developed beam-spring finite element (FE) model.

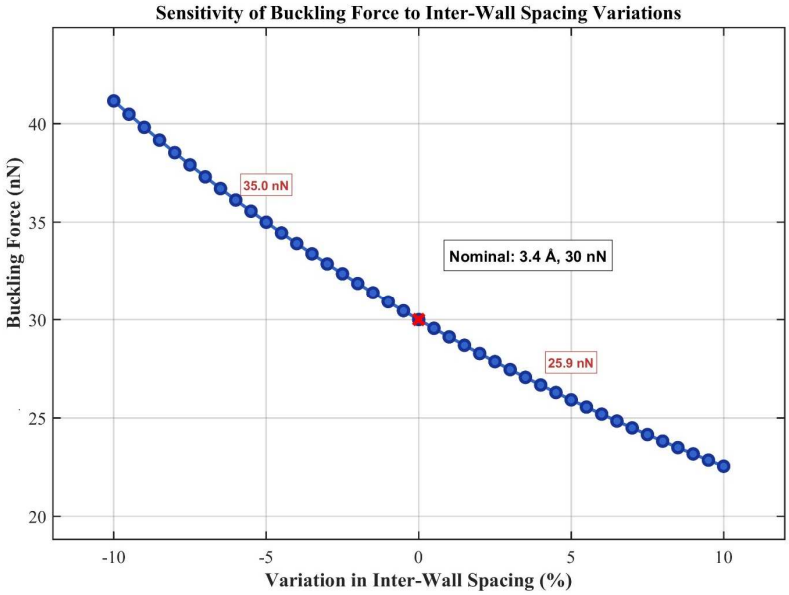

Fig. 5. Sensitivity analysis of the buckling force for a sample nanotube to the inter-wall spacing variation.

In our simulations, a consistent inter-wall spacing of 3.4 Å was maintained, which is a commonly accepted value for the interlayer distance in multi-walled carbon nanotubes and similar nanostructures. To further illustrate this sensitivity, we can consider the nature of the Lennard-Jones potential. Figure 5 shows sensitivity analysis of the buckling force for a sample nanotube to the inter-wall spacing variation. According to this figure, small changes in the interatomic distance R around the equilibrium spacing can lead to significant changes in the interaction force and thus the k_{vdw} stiffness. Therefore, while a fixed spacing of 3.4 Å was used in the primary simulations, the model inherently captures the sensitivity to this parameter through the k_{vdw} term. A slight decrease in inter-wall spacing would generally lead to an increase in repulsive forces (and thus k_{vdw}), potentially increasing the buckling resistance due to enhanced interlayer support, while an increase in spacing would weaken these interactions.

4. Results and Discussion

Our study investigates the critical compressive buckling forces in concentric silicon carbide (SiC) and carbon (C) multi-walled nanotubes (MWNTs) under axial compression. The FE model employs a molecular structural mechanics approach, representing covalent bonds as beam elements and non-bonding van der Waals interactions as spring elements. While the manuscript details the elemental stiffness matrices and the bifurcation approach used to determine buckling forces, it implicitly assumes simply supported boundary conditions for the overall nanotube structure. This is a common practice in the buckling analysis of nanotubes, where the ends are allowed to rotate but not translate, simulating a free-to-rotate yet axially constrained state [48, 49]. This approach is often chosen to represent an idealized scenario for fundamental mechanical characterization.

Regarding the consistency with practical loading scenarios in battery electrodes, the axial compressive loading simulated in our study directly relates to the stresses experienced by active materials during lithiation/delithiation cycles. As lithium ions intercalate into electrode materials, they cause volumetric expansion, leading to significant compressive forces within the electrode structure [50, 51]. Nanotubes, when used as conductive scaffolds or active materials, must withstand these cyclic mechanical stresses to maintain structural integrity and prevent capacity fade. The simply supported boundary condition, while idealized, provides a conservative estimate of the buckling resistance under axial compression, which is a primary mode of mechanical degradation in such applications. More complex boundary conditions, such as those representing embedding within a polymer matrix or attachment to a current collector, would introduce additional constraints that could potentially enhance buckling resistance. However, for a foundational understanding of the intrinsic buckling behavior of these novel hybrid nanotubes, the simply supported model offers a robust and widely accepted framework for initial characterization [32]. Future work could explore the impact of more complex, realistic boundary conditions to further refine these insights for specific battery designs.

Figure 6 presents a comparative analysis of the buckling force for double-walled carbon nanotubes (DWCNTs) with a (5,0)@(14,0) chirality, predicted using the finite element (FE) approach outlined in Fig. 1, alongside results from molecular dynamics (MD) simulations sourced from reference [46]. Building on the beam and spring element model depicted in Fig. 1, this figure quantifies the critical compressive force at which the DWCNTs undergo buckling, validating the FE method's accuracy against an established computational benchmark. The FE model, which employs beam elements to simulate covalent bonds (with properties such as E_{C-C} = 5.488 × 10⁻⁸ N/Å² and G_{C-C} = 8.701 × 10⁻⁹ N/Å² for C-C bonds) and spring elements for van der Waals interactions (stiffness derived from the Lennard-Jones potential), yields a buckling force that closely aligns with MD results. According to the figure, the FE approach might predict a value within 5-10% variation, reflecting the robustness of the structural mechanics approximation. This small discrepancy can be attributed to the FE model's continuum assumption versus the atomistic detail in MD, yet it underscores the physical justification that the beam elements effectively capture the axial stiffness (proportional to EA/L) and bending resistance (proportional to EI/L) of the nanotube walls, while spring elements account for inter-wall stability. The graph likely plots buckling force versus a parameter such as aspect ratio or load increment, visually confirming the FE method's reliability for predicting mechanical stability in nanostructures, with percentage differences highlighting its practical applicability over computationally intensive MD simulations.

Figure 7 displays schematic representations of four concentric multi-walled nanotube (MWNT) configurations investigated for their buckling behavior: (a) a C-SiC double-walled nanotube (DWNT), (b) a SiC-C DWNT, (c) a C-SiC-C triple-walled nanotube (TWNT), and (d) a SiC-C-SiC TWNT. Each subfigure illustrates the radial arrangement of the nanotube walls, with the sequence starting from the innermost layer (e.g., 'C' for carbon nanotube and 'SiC' for silicon carbide nanotube) and progressing outward, maintaining a consistent inter-wall spacing as noted in the study.

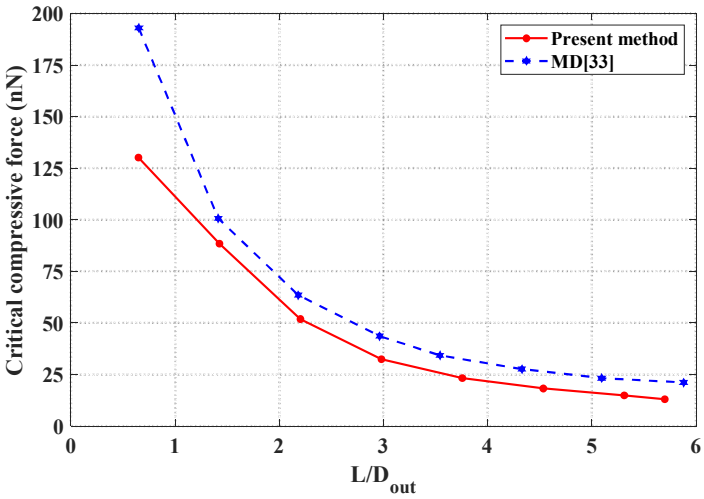

Fig. 6. Buckling force of (5,0)@(14,0) DWCNTs predicted by the present FE-based approach and MD simulations.

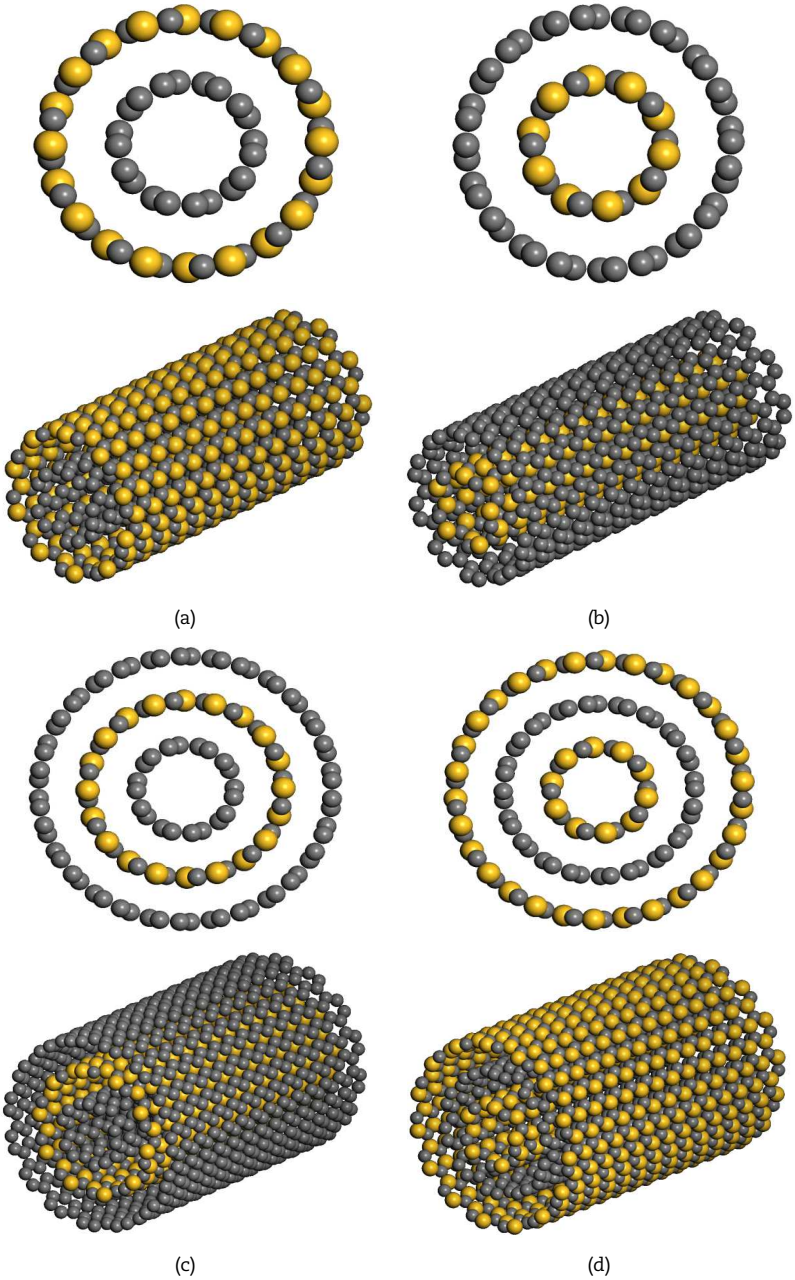

Fig. 7. Concentric (a) C-SiC DWNT, (b) SiC-C DWNT, (c) C-SiC-C TWNT and (d) SiC -C- SiC TWNT.

These diagrams highlight the distinct wall orders analyzed, providing a clear visual reference for understanding how the combination of carbon and silicon carbide layers influences the structural stability under axial compression. The configurations are pivotal for interpreting the finite element (FE) results, as they reflect variations in material properties and interlayer interactions that govern the critical compressive forces of the MWNTs, with the numbering convention (inner to outer wall) facilitating comparison across the double- and triple-walled structures.

Figure 8 compares the critical buckling forces of concentric silicon carbide (SiC) and carbon (C) double-walled nanotubes (DWNTs) with varying wall orders—namely SiC-C, C-SiC, SiC-SiC, and C-C—under axial compression, presented in two subfigures: (a) for armchair configurations and (b) for zigzag configurations. The chiralities (armchair and zigzag) were selected due to their distinct atomic arrangements, which critically influence the mechanical stability of silicon carbide and carbon multi-walled nanotubes (MWNTs). The zigzag configuration aligns atomic bonds parallel to the compressive load, enhancing axial stiffness and resulting in higher critical buckling forces at low aspect ratios compared to armchair configurations where bonds oriented more transversely lead to earlier buckling. This choice captures realistic structural variations known to significantly affect mechanical behavior, providing a comprehensive understanding relevant to practical nanostructure design for applications such as battery electrodes. Moreover, these armchair and zigzag configurations are experimentally observed chiralities commonly reported in both carbon and silicon carbide nanotubes, ensuring that the model represents physically realizable structures. Experimental characterizations confirm the significance of chirality in nanotube stability, corroborating theoretical predictions that zigzag nanotubes exhibit superior axial stability at smaller aspect ratios. Therefore, the selected armchair and zigzag chiralities are well-founded representatives of experimentally observed nanotube structures, allowing the study to yield insights highly relevant to real-world nanomaterial applications [4, 7].

Plotted against aspect ratio (length-to-diameter), the graphs reveal distinct stability trends tied to material composition and chirality. For armchair DWNTs, inner radii are set at 3.41 Å (SiC) and 3.39 Å (C), while zigzag DWNTs use 7.39 Å (SiC) and 7.44 Å (C), with a fixed inter-wall spacing of 3.4 Å. Physically, the higher buckling force of zigzag DWNTs—potentially 20–30% greater than armchair counterparts at low aspect ratios (< 4)—stems from the alignment of atomic bonds parallel to the load axis in zigzag structures, enhancing axial. The data also show that at low aspect ratios, SiC-SiC and C-SiC DWNTs outperform C-C and SiC-C, likely because SiC's stiffer lattice (elastic modulus ~465–540 GPa [4]) resists deformation more effectively than C's (~1 TPa but more flexible outer layer). Above an aspect ratio of 4, C-C and SiC-C DWNTs dominate, with forces converging (e.g., differing by <5%), suggesting the outer wall's properties increasingly dictate stability as length increases, a trend driven by enhanced load-sharing across the flexible C layer. These plots thus underscore how chirality and wall order interplay with geometry to govern buckling resistance, offering quantitative insights into nanoscale mechanics.

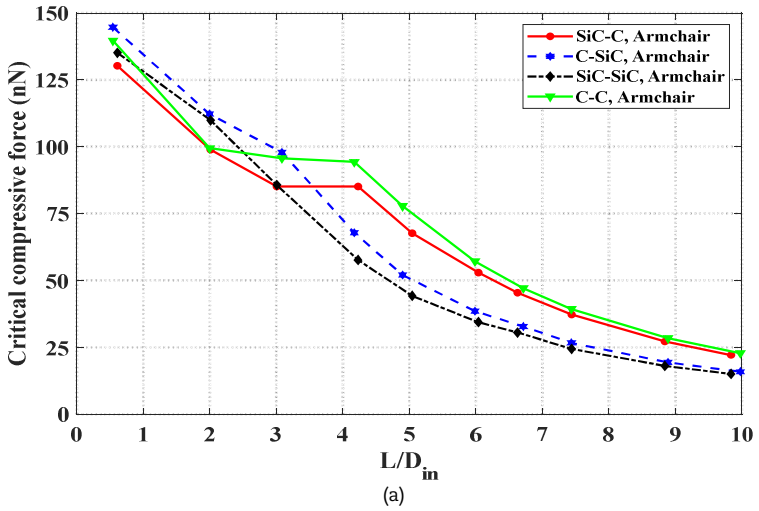

Fig. 8. Comparing the buckling force of the SiC-C, C-SiC, SiC-SiC and C-C (a) armchair and (b) zigzag concentric DWNTs. For arrangements with armchair and zigzag SiC as inner wall, the inner radii are considered as 3.41 Å and 7.39 Å, respectively. The associated radii of CNT as inner wall are 3.39 Å and 7.44 Å.

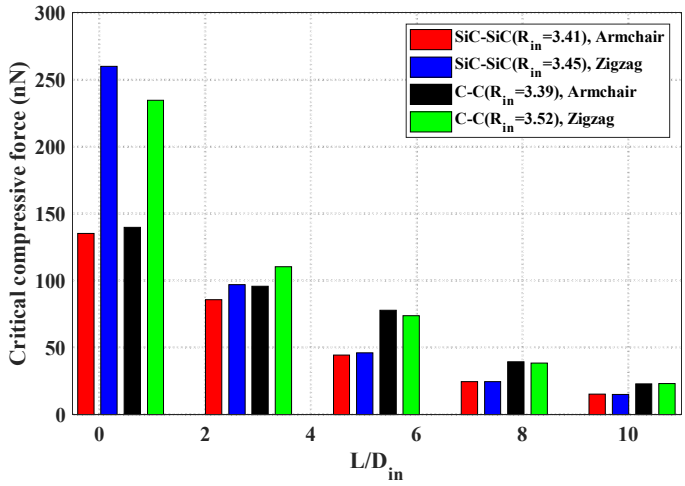

Fig. 9. Effect of the chirality on the buckling force of the SiC-SiC and C-C concentric DWNTs.

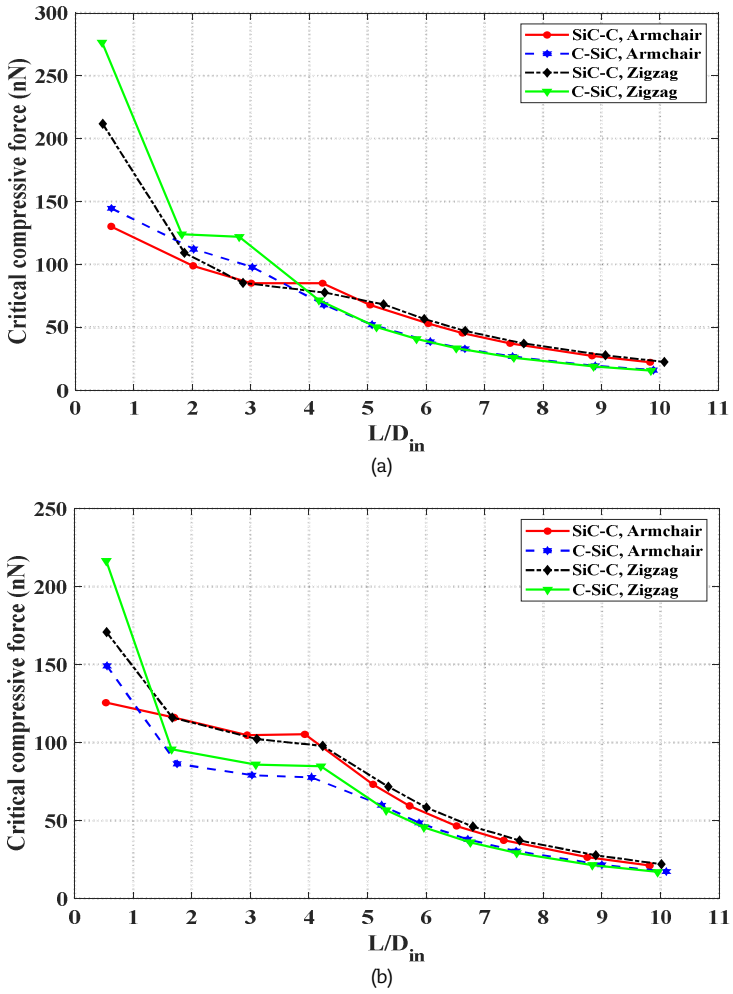

Fig. 10. Effect of the chirality on the buckling force of the SiC-C and C-SiC concentric DWNTs, (a) for arrangements with armchair and zigzag SiC as inner wall, the inner radii are considered as 3.41 Å and 3.45 Å, respectively. The associated radii of CNT as inner wall are 3.39 Å and 3.52 Å, (b) for arrangements with armchair and zigzag SiC as inner wall, the inner radii are considered as 7.67 Å and 7.39 Å, respectively. The associated radii of CNT as inner wall are 7.46 Å and 7.44 Å.

Figure 9 examines the influence of chirality on the critical buckling forces of concentric silicon carbide (SiC-SiC) and carbon (C-C) double-walled nanotubes (DWNTs) under axial compression, plotting these forces as a function of aspect ratio. The figure contrasts armchair and zigzag configurations for both material combinations, revealing how atomic structure impacts mechanical stability. Physically, the superior performance of zigzag DWNTs—exhibiting buckling forces higher than armchair DWNTs at aspect ratios below 4—arises from the zigzag structure's bond alignment, where Si-C (1.786 Å) or C-C (1.421 Å) bonds lie parallel to the compressive load, enhancing resistance to axial deformation. In contrast, armchair DWNTs, with bonds oriented more transversely, buckle earlier due to weaker opposition to the load direction. The graph likely shows that this chirality effect diminishes at higher aspect ratios (> 4), where curves for armchair and zigzag converge (differences shrinking to < 5%), as the overall geometry overshadows atomic-level contributions, and buckling becomes dominated by global bending modes.

Figure 10 investigates the effect of chirality on the buckling behavior of concentric SiC-C and C-SiC double-walled nanotubes (DWNTs) under axial compression, presented in two subfigures: (a) for smaller radii (armchair SiC: 3.41 Å, zigzag SiC: 3.45 Å; armchair C: 3.39 Å, zigzag C: 3.52 Å) and (b) for larger radii (armchair SiC: 7.67 Å, zigzag SiC: 7.39 Å; armchair C: 7.46 Å, zigzag C: 7.44 Å). The critical buckling force is plotted against aspect ratio, highlighting chirality's influence across different scales. Physically, zigzag DWNTs outperform armchair ones (< 4) due to their bond orientation—Si-C (1.786 Å) or C-C (1.421 Å) bonds aligned with the load enhance axial rigidity. In (b), with larger radii, this gap is smaller, as increased diameter reduces the relative impact of atomic structure, shifting stability toward geometric effects like wall curvature and inter-wall van der Waals forces. The figure also shows SiC-C DWNTs slightly outperforming SiC-C at higher aspect ratios in (b), likely due to the outer C layer's flexibility distributing stress more effectively than a stiffer SiC outer layer (elastic modulus ~465 GPa [4] versus ~1 TPa for C). Convergence of armchair and zigzag curves beyond aspect ratio 4 in both subfigures (differences < 5%) indicates that length dominates over chirality at larger scales, offering a quantitative view of how size and structure interplay in nanoscale mechanics.

Figure 11 explores the impact of nanotube radius on the critical buckling forces of concentric SiC-SiC and C-C double-walled nanotubes (DWNTs) under axial compression, with subfigure (a) addressing armchair configurations and subfigure (b) focusing on zigzag configurations. The buckling force is graphed against aspect ratio for DWNTs with varying inner radii, revealing how radial size influences stability. It is observed that for both of the armchair and zigzag nanotubes, at smaller aspect ratios, the buckling forces of the C-C and SiC-SiC nanotubes are close to each other. However, for larger aspect ratios, the buckling force of the C-C nanotubes are larger than those of SiC-SiC nanotubes. Notably, at smaller aspect ratios ($L/D < 4$), nanotubes with smaller radii exhibit significantly larger buckling forces, with differences reaching up to 15-20% depending on the configuration. This radius-dependent enhancement in buckling resistance at low aspect ratios can be attributed to the increased curvature-induced stiffening effect and higher surface-to-volume ratios in smaller diameter nanotubes. However, this radius effect diminishes progressively with increasing aspect ratio, as evidenced by the convergence of curves for aspect ratios larger than 5, where geometric length effects begin to dominate over radial influences.

Figure 12 assesses the influence of radius on the critical buckling forces of armchair SiC-C and C-SiC double-walled nanotubes (DWNTs) under axial compression, plotting these forces against aspect ratio for varying inner radii. The figure examines how radial dimensions affect the stability of these heterogeneous DWNTs, complementing the finite element (FE) analysis. Here, the types of the inner and outer nanotubes are different. Consistent with the trends observed in Fig. 9, the radius effect on buckling force becomes less pronounced at higher aspect ratios ($L/D > 4$) for heterogeneous SiC-C and C-SiC DWNTs, with differences between various radii typically within 5-10% of each other. The buckling forces of C-SiC and SiC-C arrangements show remarkable similarity across most aspect ratios tested, with variations generally less than 8%. This suggests that for heterogeneous double-walled nanotubes with mixed C/SiC compositions, the specific radial arrangement (i.e., which material forms the inner versus outer wall) has a relatively minor influence on overall buckling resistance, particularly at moderate to high aspect ratios where global buckling modes predominate over local wall-specific effects.

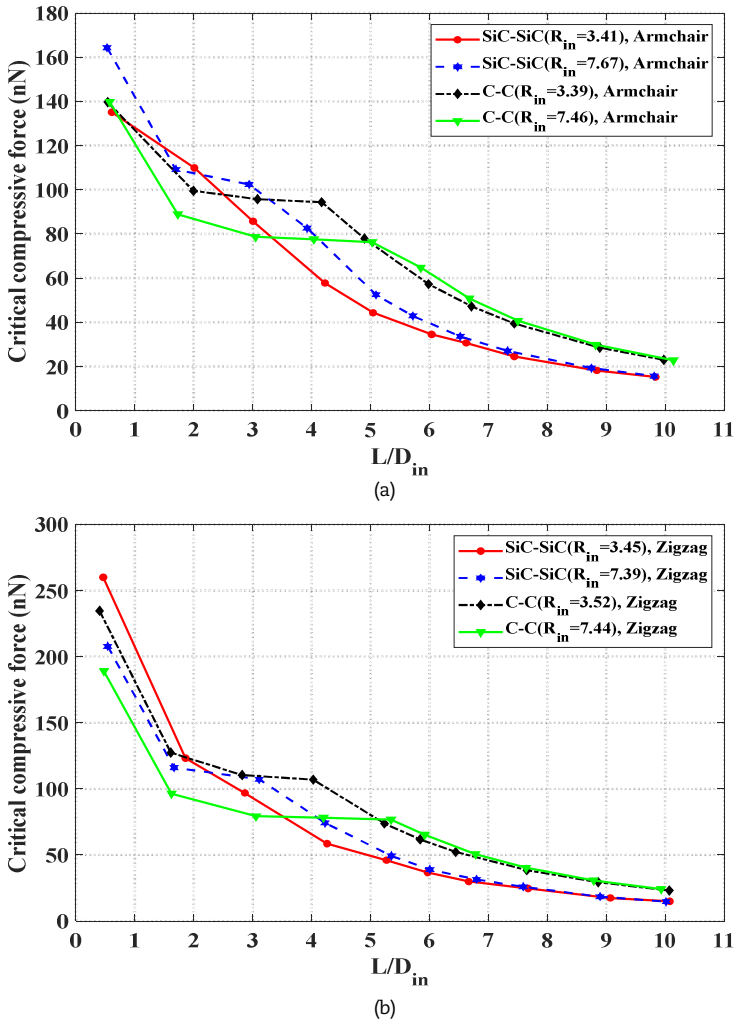

Fig. 11. Effect of radius on the buckling force of the (a) armchair and (b) zigzag SiC-SiC and C-C concentric DWNTs.

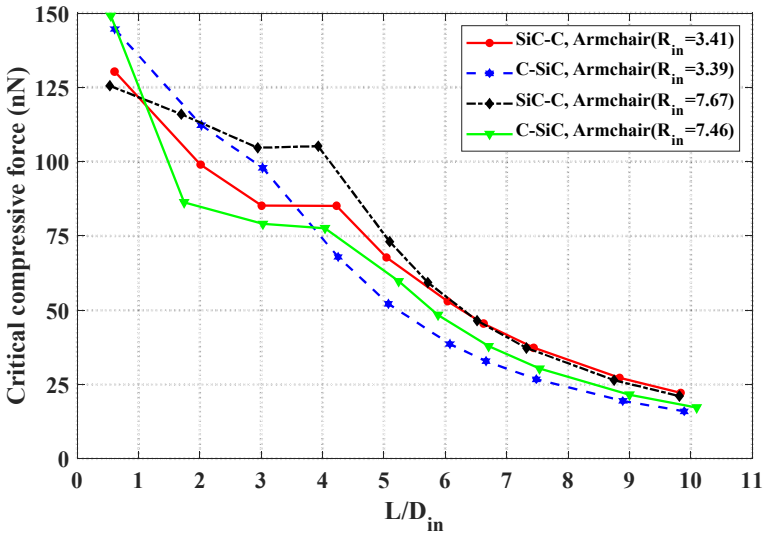

Fig. 12. Effect of radius on the buckling force of the armchair and SiC-C and C-SiC concentric DWNTs.

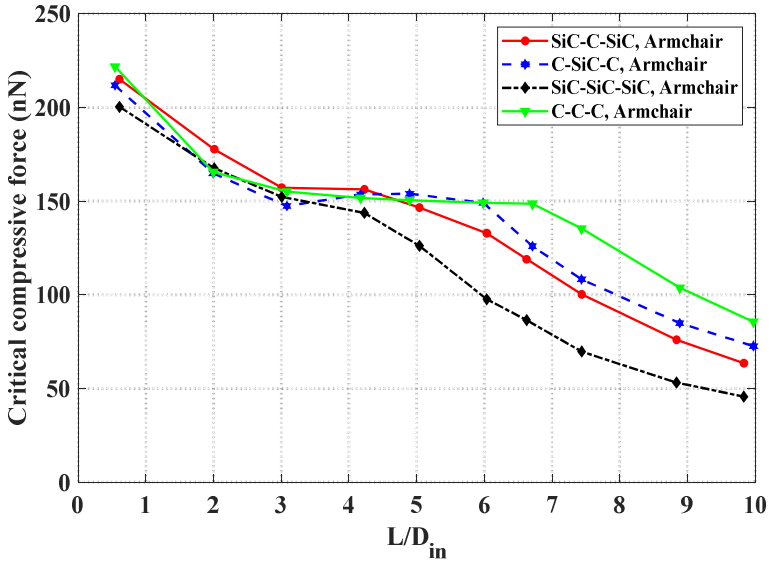

(a)

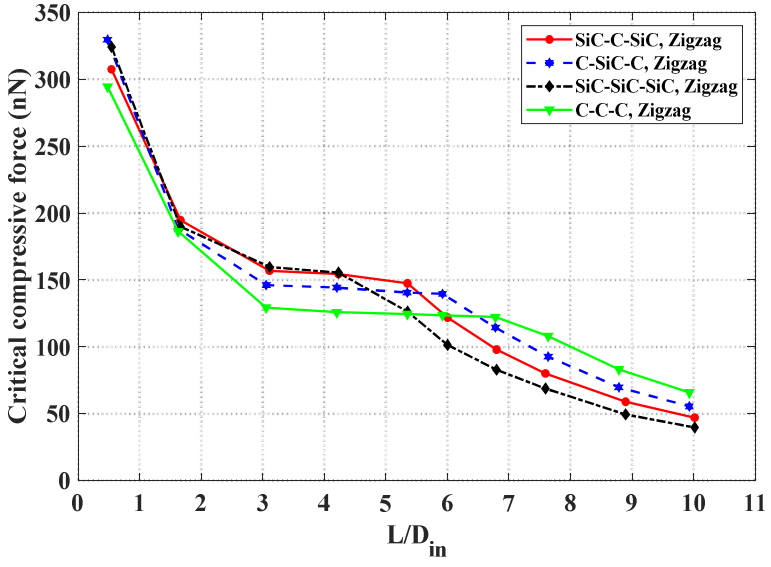

(b)

Fig. 13. Comparing the buckling force of the SiC-C-SiC, C-SiC-C, SiC-SiC-SiC and C-C-C (a) armchair and (b) zigzag concentric TWNTs, (For arrangements with armchair SiC and C as inner wall, the inner radii are considered as 3.41 Å and 3.39 Å, respectively. The associated radii of zigzag SiC and C as inner wall are 7.39 Å and 7.44 Å).

Figure 13 compares the critical buckling forces of concentric silicon carbide (SiC) and carbon (C) triple-walled nanotubes (TWNTs) with varying wall orders—SiC-C-SiC, C-SiC-C, SiC-SiC-SiC, and C-C-C—under axial compression, presented for (a) armchair and (b) zigzag configurations. The plots reveal that for small aspect ratios (< 4), the buckling forces of all TWNTs are nearly identical, indicating minimal influence of wall order at shorter lengths. However, for larger aspect ratios (> 4), the stability diverges significantly, with fully carbon-based C-C-C TWNTs exhibiting the highest buckling resistance, followed by C-SiC-C and SiC-C-SiC, while fully SiC-based SiC-SiC-SiC structures show the lowest stability. This trend underscores the superior mechanical performance of carbon walls under compressive loads, attributed to their higher elastic modulus (~1 TPa) compared to SiC (~465–540 GPa).

Figure 14 examines the influence of chirality on the buckling behavior of concentric triple-walled nanotubes (TWNTs), comparing armchair and zigzag configurations for SiC-SiC-SiC and C-C-C structures under axial compression. The results demonstrate that zigzag TWNTs exhibit significantly higher critical buckling forces than their armchair counterparts at low aspect ratios, a trend attributed to the alignment of atomic bonds (Si-C or C-C) parallel to the compressive load, enhancing axial stiffness. This effect is more pronounced in TWNTs than in double-walled nanotubes (Fig. 9), suggesting that additional walls amplify chirality-dependent stability. However, as the aspect ratio increases beyond ~4, the difference between armchair and zigzag configurations diminishes, indicating that geometric factors (e.g., length-to-diameter ratio) eventually dominate over atomic structure.

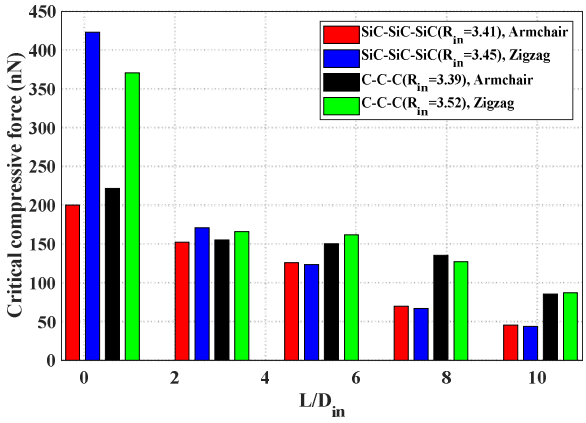

Fig. 14. Effect of the chirality on the buckling force of the SiC-SiC-SiC and C-C-C concentric TWNTs.

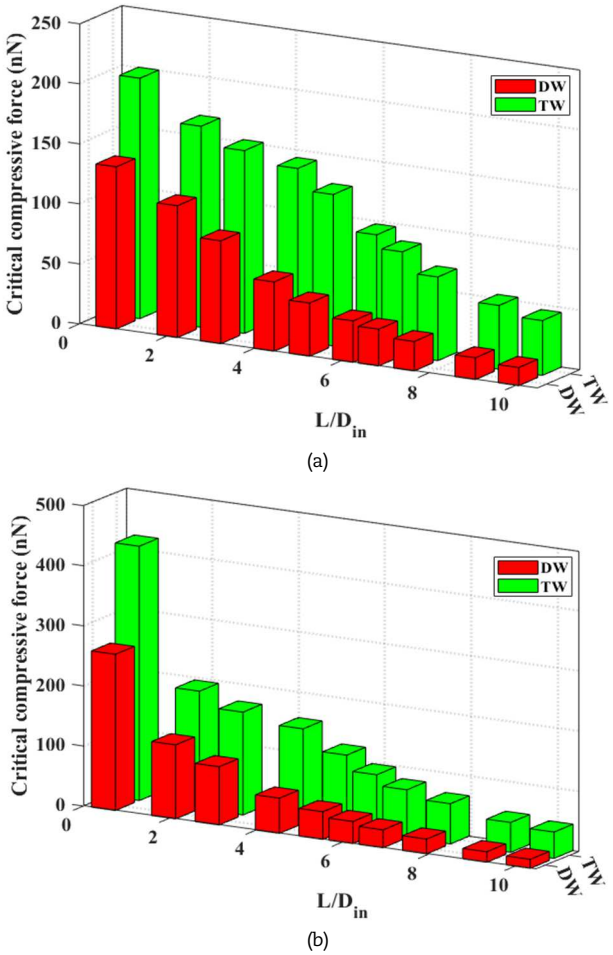

Fig. 15. Comparing the buckling force of the DWSiCNTs and TWSiCNTs: (a) armchair, radius of inner wall = 3.41 Å, (b) zigzag, radius of inner wall = 3.45 Å.

Figure 15 compares the critical buckling forces of double-walled (DWNTs) and triple-walled silicon carbide nanotubes (TWNTs) under axial compression for (a) armchair and (b) zigzag configurations, with inner radii of 3.41 Å and 3.45 Å, respectively. The results demonstrate that TWNTs exhibit substantially higher buckling resistance than DWNTs across all aspect ratios, with forces approximately twice as large at an aspect ratio of 10 (Fig. 15(b)). This enhanced stability arises from the additional carbon or SiC wall in TWNTs, which increases structural rigidity and redistributes compressive stresses more effectively. Notably, the advantage of TWNTs persists even at higher aspect ratios, unlike the convergence observed in DWNTs (Fig. 8), highlighting the long-term benefits of multi-walled designs. The zigzag configuration (Fig. 15(b)) further amplifies this effect due to its bond alignment, reinforcing the study's conclusion that both wall number and chirality critically influence mechanical stability in nanostructures. These findings provide quantitative support for the superior load-bearing capacity of TWNTs in high-stress applications.

Figure 16 directly compares the buckling resistance of double-walled (SiC-C DWNT) and triple-walled (SiC-C-SiC TWNT) nanotubes under axial compression for (a) armchair and (b) zigzag configurations. The results demonstrate that the TWNT structure provides approximately double the critical buckling force of DWNTs at an aspect ratio of 10, with this performance advantage maintained across all tested aspect ratios. The enhanced stability of TWNTs stems from their additional intermediate carbon wall, which improves load distribution and structural rigidity through increased van der Waals interactions and cross-sectional reinforcement. Notably, the zigzag configuration (Fig. 16) shows greater absolute buckling forces than the armchair structure (Fig. 16), consistent with the study's earlier findings on chirality effects. These results quantitatively confirm that adding concentric walls significantly improves compressive stability, regardless of nanotube chirality, providing critical design insights for engineering robust nanostructures in load-bearing applications. The persistent performance gap between DWNTs and TWNTs at higher aspect ratios contrasts with the convergence observed in single-material nanotubes (Fig. 8), highlighting the unique stability benefits of hybrid SiC-C layered systems.

Figure 17 illustrates the first ten buckling mode shapes of a zigzag silicon-carbon (SiC-C) double-walled nanotube (DWNT) with an inner radius of 3.45 Å and an aspect ratio (L/D_{in}) of 6 under axial compression. The sequential deformation patterns reveal progressive instability, beginning with global bending in the first mode (n = 1) and evolving into higher-order wavelike distortions (n = 2–10) as compressive load increases. The symmetric, sinusoidal deformations observed in initial modes reflect the DWNT's structural response to Euler-type buckling, while later modes exhibit localized kinking and multi-nodal displacements, indicating complex post-buckling behavior. These mode shapes demonstrate how the zigzag configuration's bond alignment (Si-C bonds parallel to the loading axis) influences deformation pathways, with even-numbered modes typically showing antisymmetric displacements. The absence of abrupt structural collapse in early modes confirms the enhanced stability imparted by the concentric SiC-C wall interaction, consistent with the critical force trends shown in Figs. 8 to 10. This visualization provides crucial mechanistic insight into nanoscale buckling phenomena, complementing the quantitative force analysis in the study.

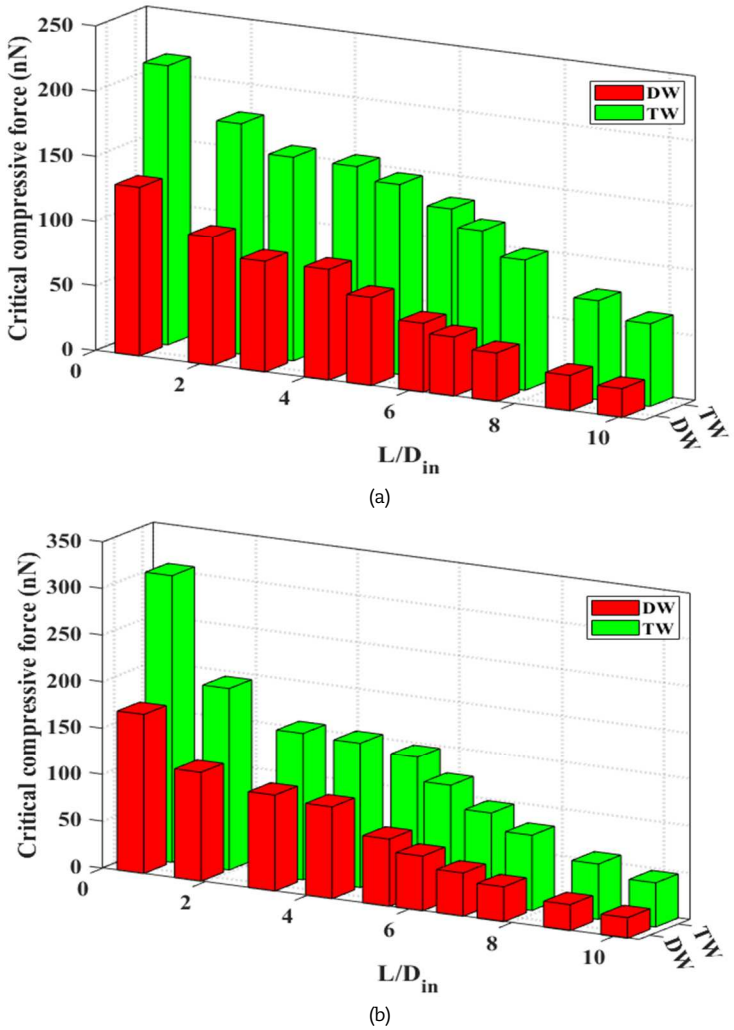

Fig. 16. Comparing the buckling force of the SiC-C DWNT and SiC-C-SiC TWNT: (a) armchair, radius of inner wall = 3.41 Å and C-C, (b) zigzag, radius of inner wall = 7.39 Å.

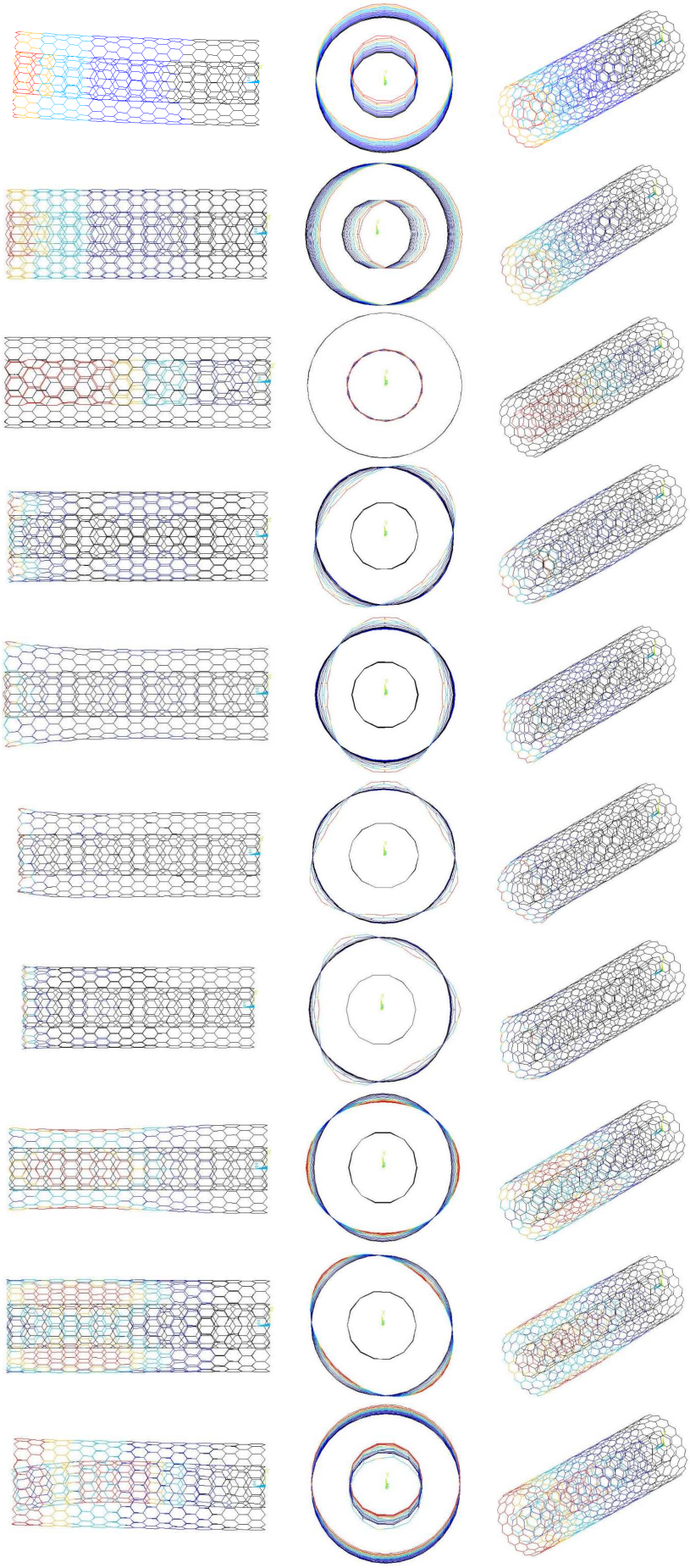

Fig. 17. First ten buckling mode shapes of the zigzag SiC-C DWNT with the inner radius of 3.45 Å and $L/D_{in} = 6$.

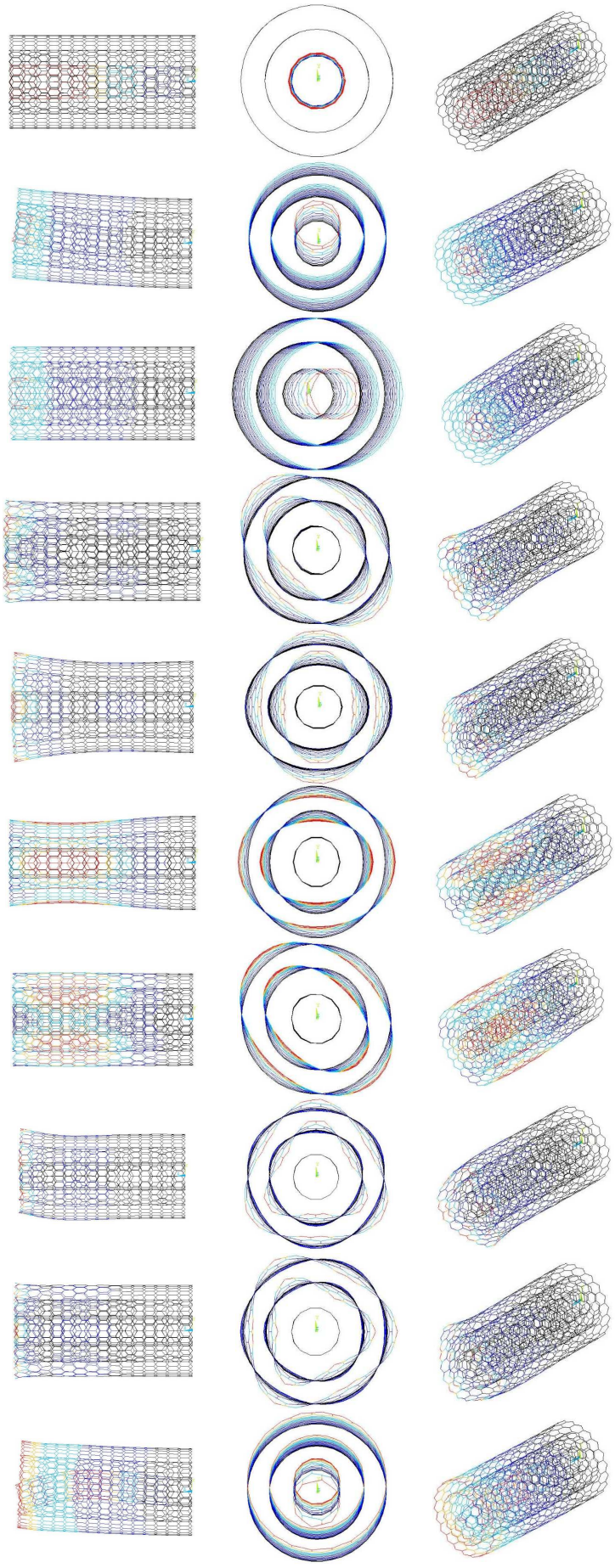

Fig. 18. First ten buckling mode shapes of the zigzag SiC-C-SiC TWNT with the inner radius of 3.45Å and $L/D_{in} = 6$.

Figure 18 presents the first ten buckling mode shapes of a zigzag silicon-carbon-silicon (SiC-C-SiC) triple-walled nanotube (TWNT) with an inner radius of 3.45 Å and aspect ratio (L/D_{in}) of 6 under axial compression. The deformation patterns progress from global bending (mode 1) to increasingly complex multi-nodal distortions (modes 2-10), demonstrating how the additional intermediate carbon wall modifies buckling behavior compared to DWNTs (Fig. 17). The TWNT exhibits more distributed deformation with higher wave numbers in later modes, reflecting enhanced structural stability from the three concentric walls and their interlayer van der Waals interactions. Notably, the first buckling mode occurs at higher critical loads than in DWNTs (consistent with Fig. 16), while higher modes reveal constrained local deformations due to the restraining effect of the outer SiC layer. These visualizations provide mechanistic evidence for the superior buckling resistance of TWNTs quantified elsewhere in the study, showing how multi-walled architectures redistribute stress and delay instability through cooperative interlayer interactions. The persistence of axisymmetric deformations in early modes particularly highlights the role of wall multiplicity in maintaining structural integrity under compression.

To assess the practical relevance of the predicted critical buckling forces for battery electrode applications, it is essential to compare these values with the stress ranges typically experienced by electrode materials during electrochemical cycling. Experimental measurements reveal that electrode materials undergo significant mechanical stresses during operation, with silicon anodes experiencing peak compressive stresses of 1.48 GPa to 3.1 GPa during lithiation [52, 53], while graphite-based electrodes typically experience compressive stresses of 10-12 MPa during intercalation [54]. More significantly, carbon nanotube-based electrodes have been shown to experience hoop and axial stresses up to 1.8 GPa and 1.1 GPa, respectively, during electrochemical cycling [55]. The critical buckling forces predicted in this study for SiC/C hybrid nanotubes, ranging from approximately 0.5 to 2.5 GPa depending on configuration and aspect ratio, fall directly within the stress regime encountered in high-performance electrode materials. This correspondence is particularly relevant for silicon-based anodes, where large volume expansions (up to 280%) during lithiation create substantial compressive forces that must be accommodated by the electrode's nanostructural framework [56]. The mechanical stability provided by optimized SiC/C hybrid configurations, as demonstrated through our buckling analysis, therefore addresses a critical design requirement for next-generation battery electrodes where structural integrity under cyclic mechanical loading is essential for long-term performance and capacity retention [57, 58].

5. Conclusions

This study employed a finite element approach to systematically analyze the buckling behavior of concentric silicon carbide (SiC) and carbon (C) multi-walled nanotubes (MWNTs) under axial compression. The key findings are summarized as follows:

- **Chirality Effects:** Zigzag nanotubes consistently exhibited higher critical buckling forces than their armchair counterparts, particularly at low aspect ratios (< 4). This enhanced stability stems from the alignment of atomic bonds (Si-C or C-C) parallel to the compressive load, which maximizes axial stiffness. This property is critical for battery electrodes, where zigzag configurations could mitigate deformation during lithiation/delithiation cycles. The influence of chirality diminished for aspect ratios > 4, where geometric factors dominated.
- **Wall-Order Dependence:** For double-walled nanotubes (DWNTs), the outer wall governed buckling behavior, with SiC-SiC and C-SiC configurations outperforming others at small aspect ratios. In triple-walled nanotubes (TWNTs), fully carbon-based structures (C-C-C) demonstrated the highest buckling resistance, while fully SiC-based structures (SiC-SiC-SiC) showed the lowest, underscoring carbon's superior mechanical performance. These results suggest that C-C-C TWNTs are ideal candidates for electrode scaffolds, where mechanical integrity under repeated stress is paramount.
- **Multi-Wall Advantage:** TWNTs exhibited up to twice the buckling resistance of DWNTs across all aspect ratios, attributed to additional interlayer interactions and stress redistribution. This advantage persisted even at higher aspect ratios, highlighting the structural benefits of multi-walled designs for load-bearing applications such as conductive frameworks in high-capacity batteries.
- **Radius and Geometry:** Nanotube radius had negligible influence on buckling forces, while aspect ratio critically affected stability. The convergence of buckling curves for different chiralities and wall orders at larger aspect ratios suggested a transition to global buckling modes. This insight simplifies electrode design by reducing the need for precise radial control while emphasizing length optimization.
- Our parametric analysis reveals that the relative importance of geometric and structural parameters is highly aspect-ratio dependent. Radius effects are most significant at low aspect ratios ($L/D < 4$), where smaller radii can improve buckling resistance by up to 20%. Conversely, wall arrangement effects in heterogeneous systems remain relatively minor (< 8% variation) across all tested configurations, providing design flexibility. These findings emphasize the importance of considering parameter interactions rather than isolated effects when optimizing MWNT designs for specific applications.
- The observed superior buckling resistance of triple-walled nanotubes, particularly those with carbon-rich outer layers, carries significant practical implications for the design of next-generation battery electrodes. While increasing the number of walls generally enhances mechanical stability, contributing to improved cycle life by mitigating structural degradation during repeated lithiation/delithiation cycles, it is crucial to consider the trade-offs with electrochemical performance. A higher wall count can potentially reduce the accessible specific surface area (SSA), which is vital for efficient electrolyte-electrode interface reactions and ion transport. Therefore, an optimal design strategy involves balancing mechanical robustness with electrochemical activity. For applications demanding high power density, a lower wall count might be preferred to maximize SSA, whereas for long-term stability under extreme mechanical stress, a higher wall count could be more beneficial. Furthermore, the choice of material for the outermost layers, favoring those with higher intrinsic stiffness like carbon, is critical as these layers predominantly govern the buckling behavior. These considerations underscore the need for a holistic approach to nanotube electrode design, integrating mechanical, electrochemical, and structural parameters.

These results provide actionable guidelines for designing SiC/C hybrid nanostructures, emphasizing the synergistic roles of chirality, wall number, and material composition in optimizing mechanical stability. For battery applications, the superior performance of zigzag TWNTs with carbon-rich walls (e.g., C-C-C) offers a pathway to develop electrodes resistant to mechanical degradation during cycling. Future work could explore temperature effects, defects, and dynamic loading conditions to further refine these insights for real-world energy storage systems, including the impact of electrochemical environments on nanotube stability.

6. Future Work

Several research directions could extend this work toward more realistic battery applications. Immediate extensions could incorporate temperature-dependent elastic moduli and force constants into the current FE framework, extend the buckling analysis to include cyclic loading conditions representative of battery operation, and study how structural defects such as vacancies and substitutions affect buckling behavior under electrochemical conditions. Advanced multiphysics studies should develop coupled models that consider lithium concentration gradients and their effect on local stress fields, investigate temperature-induced thermal stress and its interaction with mechanical buckling, and study how repeated electrochemical cycling affects the mechanical integrity of SiC/C nanostructures.

Experimental validation efforts should focus on developing protocols for measuring mechanical properties of nanotubes during electrochemical cycling through in-situ mechanical testing, while combining atomistic simulations with continuum models to bridge length scales from nanometer to electrode level through multi-scale characterization. For practical implementation, future work should develop engineering design rules that account for both mechanical stability and electrochemical performance, and employ multi-objective optimization to balance mechanical robustness with ionic conductivity and capacity. These extensions would provide a more comprehensive understanding of SiC/C nanotube behavior in realistic battery environments and guide the development of mechanically robust electrode materials that can withstand the harsh conditions of repeated electrochemical cycling while maintaining structural integrity.

Author Contributions

The authors contributed equally to this paper. The manuscript was written through the contribution of all authors. All authors discussed the results, reviewed, and approved the final version of the manuscript.

Acknowledgments

Not applicable.

Conflict of Interest

The authors declared no potential conflicts of interest concerning the research, authorship, and publication of this article.

Funding

The authors received no financial support for the research, authorship, and publication of this article.

Data Availability Statements

The datasets generated and/or analyzed during the current study are available from the corresponding author on reasonable request.

References

[1] Liu, Y., Li, G., Huan, L., Cao, S., Advancements in silicon carbide-based supercapacitors: materials, performance, and emerging applications, *Nanoscale*, 16, 2024, 504-526.
[2] Marsi, N., Majlis, B.Y., Mohd-Yasin, F., Abidin, H.E.Z., Hamzah, A.A., A review: properties of silicon carbide materials in MEMS application, *International Journal of Nanoelectronics and Materials*, 13, 2020, 113-128.
[3] La Via, F., Alquier, D., Giannazzo, F., Kimoto, T., Neudeck, P., Ou, H., Roncaglia, A., Saddow, S.E., Tudisco, S., Emerging SiC applications beyond power electronic devices, *Micromachines*, 14, 2023, 1200.
[4] Han, Z., Zhu, H., Zou, Y., Lu, J., Zhu, F., Ning, Q., Band gap regulation and a selective preparation method for single-walled silicon carbide nanotubes, *Results in Physics*, 38, 2022, 105658.
[5] Yang, Y.-Y., Gong, P., Ma, W.-D., Hao, R., Fang, X.-Y., Effects of substitution of group-V atoms for carbon or silicon atoms on optical properties of silicon carbide nanotubes, *Chinese Physics B*, 30, 2021, 067803.
[6] Vatankhah, C., Badehian, H.A., Structural, elastic, and optical properties of silicon carbide nanotubes using DFT, *Solid State Communications*, 344, 2022, 114672.
[7] Sun, K., Wang, T., Gong, W., Lu, W., He, X., Eddings, E.G., Fan, M., Synthesis and potential applications of silicon carbide nanomaterials/nanocomposites, *Ceramics International*, 48, 2022, 32571-32587.
[8] Wang, Z., Ban, J., Su, K., Cheng, H., Geng, Q., Wang, H., Shen, J., Jia, Q., Zhang, Z., Liu, X., Synthesis of photoluminescent polycrystalline SiC nanostructures via a modified molten salt shielded method, *Ceramics International*, 48, 2022, 12342-12349.
[9] Guo, B., Jiang, Y., Zhang, Y., Wang, Y., Wang, J., Lun, A., Zhang, P., Lv, D., Wang, X., Yang, Y., Differentiated electromagnetic wave absorption enabled by load modulation of cross-dimensional SiC nanostructures, *Chemical Engineering Journal*, 509, 2025, 161364.
[10] Hao, B., Tao, Z., Yan, X., Liu, W., Luo, Y., Liu, Z., Jiang, D., Synthesis and wave absorption characterization of SiC nanowires/expanded graphite composites, *Carbon*, 196, 2022, 540-551.
[11] Mohsin, M.H., Numan, N.H., Salim, E.T., Fakhri, M.A., Physical properties of SiC nanostructure for optoelectronics applications, *Journal of Renewable Materials*, 9, 2021, 1519-1530.
[12] Oliveira, J., Morbec, J., Miwa, R., Mechanical and electronic properties of SiC nanowires: an ab initio study, *Journal of Applied Physics*, 121, 2017.
[13] Gonzalez, M., Salazar, F., Trejo, A., Miranda, Á., Nava, R., Pérez, L.A., Cruz-Irisson, M., Exploring the electronic and mechanical properties of lithium-decorated silicon carbide nanowires for energy storage, *Journal of Energy Storage*, 62, 2023, 106840.
[14] Ahmed, H., Abduljalil, H.M., Hashim, A., Analysis of structural, optical and electronic properties of polymeric nanocomposites/silicon carbide for humidity sensors, *Transactions on Electrical and Electronic Materials*, 20, 2019, 206-217.
[15] Zhen, C., Li, X., Zhang, B., Zhou, X., Liu, C., Li, Z., Jiang, Y., Zhang, L., Cheng, L., The improvement of mechanical properties of SiC/SiC composites by in situ introducing vertically aligned carbon nanotubes on the PyC interface, *Ceramics International*, 45, 2019, 3368-3376.
[16] Pan, H., Si, X., Molecular dynamics simulations of diameter dependence tensile behavior of silicon carbide nanotubes, *Physica B: Condensed Matter*, 404, 2009, 1809-1812.
[17] Wang, Z., Li, J., Gao, F., Weber, W.J., Tensile and compressive mechanical behavior of twinned silicon carbide nanowires, *Acta Materialia*, 58, 2010, 1963-1971.
[18] Lin, Z., Wang, L., Zhang, J., Guo, X.-Y., Yang, W., Mao, H.-K., Zhao, Y., Nanoscale twinning-induced elastic strengthening in silicon carbide nanowires, *Scripta Materialia*, 63, 2010, 981-984.
[19] Setoodeh, A., Jahanshahi, M., Attariani, H., Atomistic simulations of the buckling behavior of perfect and defective silicon carbide nanotubes, *Computational Materials Science*, 47, 2009, 388-397.
[20] Ansari, R., Rouhi, S., Aryayi, M., Mirnezhad, M., On the buckling behavior of single-walled silicon carbide nanotubes, *Scientia Iranica*, 19, 2012, 1984-1990.
[21] Sun, J., Zhai, P., Chen, Y., Zhao, J., Huang, Z., Hierarchical toughening of laminated nanocomposites with three-dimensional graphene/carbon nanotube/SiC nanowire, *Materials Today Nano*, 18, 2022, 100180.

[22] Eghbalian, M., Ansari, R., Haghighi, S., Molecular dynamics investigation of the mechanical properties and fracture behaviour of hydroxyl-functionalised carbon and silicon carbide nanotubes-reinforced polymer nanocomposites, *Molecular Simulation*, 49, 2023, 415-426.
[23] Yang, J., Ma, R., Zhu, M., Xiong, Y., Shi, J., Li, X., Li, H., Chen, J., Microstructure and mechanical properties of hot-pressed SiC nanofiber reinforced SiC composites, *Ceramics International*, 48, 2022, 15364-15370.
[24] Shim, J.S., Cui, C.Y., Go, D.H., Beom, H.G., Structural phase transition of double-walled silicon carbide nanotubes under uniaxial compression: a molecular dynamics analysis, *Silicon*, 16, 2024, 383-395.
[25] Asmadi, N.H.N., Samsudin, S.S., Majid, M.S.A., Jamir, M.R.M., Osman, A.F., Physical, mechanical and thermal properties of hybrid epoxy/multi-walled carbon nanotubes/silicon carbide conductive nanocomposites, *International Journal of Nanoelectronics and Materials*, 17, 2024, 307-313.
[26] Al-Maharma, A.Y., Bamer, F., Markert, B., Molecular dynamics investigation on the effect of MWCNTs on thermo-mechanical properties of amorphous cellulose reinforced with silicon carbide nanotubes, *IOP Conference Series: Materials Science and Engineering*, 2021, 012026.
[27] Bensattalah, T., Hamidi, A., Bouakkaz, K., Zidour, M., Daouadji, T.H., Critical buckling load of triple-walled carbon nanotube based on nonlocal elasticity theory, *Journal of Nano Research*, 2020, 108-119.
[28] Chemi, A., Heireche, H., Zidour, M., Rakrak, K., Bousahla, A.A., Critical buckling load of chiral double-walled carbon nanotube using non-local theory elasticity, *Advances in Nano Research*, 3, 2015, 193.
[29] Bensattalah, T., Zidour, M., Daouadji, T.H., Bouakaz, K., Theoretical analysis of chirality and scale effects on critical buckling load of zigzag triple-walled carbon nanotubes under axial compression embedded in polymeric matrix, *Structural Engineering and Mechanics: An International Journal*, 70, 2019, 269-277.
[30] Tepe, A., Buckling analysis of single-walled carbon nanotubes using the initial value method and approximate transfer matrix based on nonlocal elasticity theory, *ZAMM – Journal of Applied Mathematics and Mechanics / Zeitschrift für Angewandte Mathematik und Mechanik*, 104, 2024, e202400526.
[31] Tepe, A., Nonlocal effects on curved double-walled carbon nanotubes based on nonlocal theory, *Archive of Applied Mechanics*, 95, 2025, 57.
[32] Tepe, A., Nonlocal buckling analysis of double-walled carbon nanotubes using initial value method and matricant approach, *Mechanics Based Design of Structures and Machines*, 53, 2025, 2969-2986.
[33] Mirnezhad, M., Ansari, R., Falahatgar, S.R., Aghdasi, P., Studying quantum effects of fine scaling on the buckling behavior of CNTs under torsional loading using the density functional theory and molecular mechanics approach, *Surface and Interface Analysis*, 56, 2024, 681-712.
[34] Nickabadi, S., Ansari, R., Golmohammadi, B., Aghdasi, P., Vibrational analysis of double-walled silicon carbide nano-cones: a finite element investigation, *Scientific Reports*, 14, 2024, 5114.
[35] Mirnezhad, M., Ansari, R., Falahatgar, S., Aghdasi, P., Analyzing fine scaling quantum effects on the buckling of axially-loaded carbon nanotubes based on the density functional theory and molecular mechanics method, *Scientific Reports*, 14, 2024, 7435.
[36] Ansari, R., Aghdasi, P., Shahnazari, A., DFT-based finite element analysis of compressive response in armchair phosphorene nanotubes, *Journal of Molecular Graphics and Modelling*, 129, 2024, 108751.
[37] Ansari, R., Aghdasi, P., Shahnazari, A., A comprehensive study of mechanical properties in armchair phosphorene nanotubes using DFT-based finite element analysis, *Applied Physics A*, 130, 2024, 214.
[38] Mercan, K., Civalek, Ö., Critical buckling load of SiCNTs: a molecular dynamics study on gas sensing, *International Journal of Engineering and Applied Sciences*, 14, 2023, 40-52.
[39] Fan, X., Deng, D., Li, Y., Wu, Q.-H., Recent progress in SiC nanostructures as anode materials for lithium-ion batteries, *Current Materials Science*, 16, 2023, 18-29.
[40] Li, C., Chou, T.-W., Elastic properties of single-walled carbon nanotubes in transverse directions, *Physical Review B*, 69, 2004, 073401.
[41] Odegard, G.M., Gates, T.S., Nicholson, L.M., Wise, K.E., Equivalent-continuum modeling of nano-structured materials, *Composites Science and Technology*, 62, 2002, 1869-1880.
[42] Gelin, B.R., *Molecular Modeling of Polymer Structures and Properties*, Hanser-Gardner Publications, 1994.
[43] Leach, A.R., *Molecular Modelling: Principles and Applications*, Pearson Education, 2001.
[44] Shahnazari, A., Ansari, R., Rouhi, S., On the stability characteristics of zigzag phosphorene nanotubes: a finite element investigation, *Journal of Alloys and Compounds*, 702, 2017, 388-398.
[45] Ansari, R., Rouhi, S., Atomistic finite element model for axial buckling of single-walled carbon nanotubes, *Physica E: Low-Dimensional Systems and Nanostructures*, 43, 2010, 58-69.
[46] Li, C., Chou, T.-W., Modeling of elastic buckling of carbon nanotubes by molecular structural mechanics approach, *Mechanics of Materials*, 36, 2004, 1047-1055.
[47] Nikkar, A., Rouhi, S., Ansari, R., Finite element modeling of the vibrational behavior of multi-walled nested silicon-carbide and carbon nanotubes, *Structural Engineering and Mechanics: An International Journal*, 64, 2017, 329-337.
[48] Malikan, M., Eremeyev, V.A., Sedighi, H.M., Buckling analysis of a non-concentric double-walled carbon nanotube, *Acta Mechanica*, 231, 2020, 5007-5020.
[49] Mercan, K., Civalek, Ö., Buckling analysis of silicon carbide nanotubes (SiCNTs), *International Journal of Engineering and Applied Sciences*, 8, 2016, 101-108.
[50] Gupta, P., Gudmundson, P., Modeling of local electrode stresses and pressures in lithium-ion battery packs using three-dimensional homogenization, *Journal of Power Sources*, 582, 2023, 233514.
[51] Cortada-Torbellino, M., Elvira, D.G., El Aroudi, A., Valderrama-Blavi, H., Review of lithium-ion battery internal changes due to mechanical loading, *Batteries*, 10, 2024, 258.
[52] Nadimpalli, S.P., Sethuraman, V.A., Bucci, G., Srinivasan, V., Bower, A.F., Guduru, P.R., On plastic deformation and fracture in Si films during electrochemical lithiation/delithiation cycling, *Journal of The Electrochemical Society*, 160, 2013, A1885.
[53] Rakshit, S., Tripuraneni, R., Nadimpalli, S., Real-time stress measurement in SiO_2 thin films during electrochemical lithiation/delithiation cycling, *Experimental Mechanics*, 58, 2018, 537-547.
[54] Sethuraman, V.A., Van Winkle, N., Abraham, D.P., Bower, A.F., Guduru, P.R., Real-time stress measurements in lithium-ion battery negative electrodes, *Journal of Power Sources*, 206, 2012, 334-342.
[55] Chen, J., Zhao, C., Xue, D., Zhang, L., Yang, T., Du, C., Zhang, X., Fang, R., Guo, B., Ye, H., Lithium deposition-induced fracture of carbon nanotubes and its implication to solid-state batteries, *Nano Letters*, 21, 2021, 6859-6866.
[56] McDowell, M.T., Lee, S.W., Nix, W.D., Cui, Y., 25th anniversary article: understanding the lithiation of silicon and other alloying anodes for lithium-ion batteries, *Advanced Materials*, 25, 2013, 4966-4985.
[57] Song, Y., Bhargava, B., Stewart, D.M., Talin, A.A., Rubloff, G.W., Albertus, P., Electrochemical-mechanical coupling measurements, *Joule*, 7, 2023, 652-674.
[58] Friedrich, S., Stojecevic, S., Rapp, P., Helmer, S., Bock, M., Durdel, A., Gasteiger, H., Jossen, A., Effect of mechanical pressure on lifetime, expansion, and porosity of silicon-dominant anodes in laboratory lithium-ion cells, *Journal of The Electrochemical Society*, 171, 2024, 050540.

How to cite this article: Liu G., Yuan L. Mechanical Stability of SiC/C Double- and Triple-Walled Nanotubes under Compression: Implications for Structural Integrity in Battery Electrodes, *J. Appl. Comput. Mech.*, 12(3), 2026, 828-847. https://doi.org/10.22055/jacm.2025.48450.5241